Engineering Geology 293 (2021) 106317

Contents lists available at ScienceDirect

Engineering Geology

journal homepage: www.elsevier.com/locate/enggeo

Stability analysis of unsaturated slopes under elevated temperatures

Sannith Kumar Thota [a,b], Farshid Vahedifard [a,*]

[a] Richard A. Rula School of Civil and Environmental Engineering, Mississippi State University, Mississippi State, MS 39762, USA
[b] Schnabel Engineering, Sterling, VA 20166, USA

ARTICLE INFO

Keywords:
Unsaturated soil
Slope stability
Temperature
Effective stress
Shear strength

ABSTRACT

Several natural and man-made phenomena (e.g., droughts, wildfires, shallow geothermal technologies) can subject unsaturated slopes to elevated temperatures. However, the impact of temperature on the stability of unsaturated slopes is not well understood. This study aims to examine the stability of unsaturated intact slopes under elevated temperatures. An analytical framework is developed to calculate the factor of safety (FOS) of unsaturated slopes under steady fluid flow conditions at various temperatures. The theoretical basis of the framework is built upon the concept that, within the temperatures range investigated, the influence of temperature on the soil's shear strength is primarily attributed to thermal induced changes in apparent cohesion stemming from matric suction. Temperature dependency of apparent cohesion is quantified by employing temperature-dependent soil-water retention curve (SWRC) and effective stress models, which are then integrated into an infinite slope stability analysis of unsaturated soils under steady flow. A saturation-dependent thermal conductivity is used to obtain the temperature profile versus depth. The formulations are used to determine FOS for intact slopes with different hypothetical soils including sand, silt, and clay at surface temperatures of 25, 40, and 55 °C under different steady flow rates. Results show that the effective stress, shear strength, and FOS increase by increasing temperature from 25 °C to 55 °C. Results reveal that the effect of temperature on the stability of clayey and silty slopes can be considerable. The proposed models are validated against two sets of laboratory-measured data from the literature. The presented model provides a simple and effective method for site-specific and regional-scale stability analyses of unsaturated slopes under different thermal and seepage conditions.

1. Introduction and background

Unsaturated slopes can be exposed to elevated temperatures due to several reasons including prolonged droughts, heatwaves, thermally active earthen systems, and shallow geo-energy technologies. For instance, the soil temperature can exceed 65 °C in man-made slopes used in municipal solid waste landfills and heat exchanger projects (Yesiller and Hanson, 2003; Coccia et al., 2013; Jafari et al., 2017). Geo-energy related applications such as high voltage buried cables subject unsaturated soil slopes to temperatures above 70 °C (Garrido et al., 2003; Salata et al., 2015). Further, several cases have been reported in the literature where the surface temperature in arid regions or under heatwaves and prolonged droughts increased as high as 50 °C, directly affecting earth structures and slopes through soil-atmospheric interaction (Kasozi et al., 2015; Lorenz et al., 2010). Record data from the past and projected data for the future demonstrate increases in the frequency and severity of heatwaves, droughts and concurrent droughts and heatwaves in several regions (Mazdiyasni and AghaKouchak, 2015; Mukherjee and Mishra, 2021; Chiang et al., 2021). All these emphasize the need to study the impact of elevated temperatures on the integrity of unsaturated slopes under a changing climate (Damiano and Mercogliano, 2013; Vardon, 2015; Vahedifard et al., 2016a, 2017, 2018a). However, the impact of temperature is yet to be understood and incorporated into the stability analysis of unsaturated slopes; an area that certainly warrants further investigation (Nishimura et al., 2009; Elia et al., 2017).

The main exchanges of mass and energy that moderate meteorological conditions take place at the soil surface. Several climatic events such as extreme precipitation and droughts are dominated by land-atmospheric interactions in which soil moisture plays an important role. Other important meteorological factors such as temperature, heat flux, wind, and relative humidity are among the other important factors that influence the water movement in near-surface soils (An et al., 2017; Tang et al., 2018; Robinson and Vahedifard, 2016; Vahedifard et al.,

* Corresponding author.
E-mail address: farshid@cee.msstate.edu (F. Vahedifard).

https://doi.org/10.1016/j.enggeo.2021.106317
Received 28 January 2021; Received in revised form 22 June 2021; Accepted 30 July 2021
Available online 3 August 2021

2015; Sedighi et al., 2018). The behavior of unsaturated zone, between the soil surface and the water table, is considerably affected by water and heat transfer between the soil and atmosphere, and through the soil surface. Hence, properly incorporating the parameters that influence the water content and suction of unsaturated soils is paramount to improving the understanding of soil slope stability.

Previous studies have demonstrated that elevated temperatures can affect micro-scale characteristics and macro-scale engineering properties of soils (Hueckel and Baldi, 1990; Uchaipichat and Khalili, 2009; Goodman and Vahedifard, 2019; McCartney et al., 2019; Vahedifard et al., 2020; Cao et al., 2021). Experimental test results reported in the literature exhibit contrasting trends on the impact of temperature on the shear strength of the soil. The first group of studies found that an increase in temperature causes weakening in soil (e.g., Mitchell, 1964; Campanella and Mitchell, 1968; Hueckel and Baldi, 1990; Kuntiwattanakul et al., 1995; Alsherif and McCartney, 2015). Hueckel and Baldi (1990) reported that an increase in temperature induced lower shear strength under drained conditions. From the drained test paths conducted on silty specimens, Alsherif and McCartney (2015) concluded that heating the soil before the application of suction can lead to a lower peak shear strength. This behavior may be due to the softening effect of heating was larger than the hardening effect of suction. On the other hand, the second group of studies has shown that an increase in temperature strengthens soil (e.g., Laguros, 1969; Houston et al., 1985; Alsherif and McCartney, 2015). Laguros (1969) measured the unconfined compressive strength of four clay soils, kaolinite, illite, montmorillonite, and montmorillonite- illite, at elevated temperatures and showed that, except for the illite soil, the soil strength increases at elevated temperature. Using a suction application before the temperature test path, Alsherif and McCartney (2015) found that the soil specimens consistently exhibit a greater peak shear strength at elevated temperatures. The above-mentioned contracting trends on the temperature impact on the strength of soil can be partly attributed to different stress histories, drainage conditions, and range of applied temperatures employed in these tests (Graham et al., 2001).

Under drained and undrained conditions, elevated temperature can alter the stability of an unsaturated slope differently. For instance, variations in temperature can increase the permeability of near surface soils facilitating seepage flow parallel to the slope and alter the factor of safety (FOS) (Greenway, 1987; Pradel and Raad, 1993; Bo et al., 2008). For undrained conditions, Uchaipichat (2017) showed that the FOS of unsaturated silty slopes decreases with increasing temperature (25 to 60 °C). Another thermal effect on unsaturated slopes is through temperature-induced change in the soil water retention curve (SWRC) and effective stress, which in turn influence the shear strength and stability of unsaturated slopes (Thota et al., 2019). Under drained conditions, elevated temperatures can increase the matric suction of the soil and hence, can increase the effective stress and shear strength of the soil (Uchaipichat and Khalili, 2009; Alsherif and McCartney, 2015). For a constant water content, previous studies have shown that an increase in temperature causes a downward shift in the SWRC, leading to a decrease in matric suction (Wan et al., 2015; Roshani and Sedano, 2016). The reduction in matric suction can decrease effective stress and the FOS. This observation is valid for undrained conditions, where the water content is constant. However, for changing water content (e.g., drained condition), the elevated temperatures cause increased evaporation and reduced water content leading to increased suction and therefore increased the FOS (Uchaipichat and Khalili, 2009).

A key step for any attempt towards analyzing the stability of unsaturated slopes lies within properly determining the shear strength of unsaturated soils. While contradictory trends are reported in the literature regarding the effect of temperature on shear strength, most experimental test results agree that elevated temperatures have minimal effects on the effective angle of friction and cohesion particularly at critical state (Lingnau et al., 1996; Hueckel et al., 1998; Burghignoli et al., 2000; Graham et al., 2001; Uchaipichat and Khalili, 2009; Mašín and Khalili, 2011; Yavari et al., 2016; Maghsoodi et al., 2019; Li et al., 2019). However, previous studies (Uchaipichat and Khalili, 2009; Wan et al., 2015; Roshani and Sedano, 2016) show that the temperature effect on matric suction and degree of saturation can be considerable.

This study aims to examine the stability of intact (i.e., uncracked) unsaturated slopes subject to elevated temperatures. An analytical framework is developed to determine the FOS of unsaturated slopes under steady fluid flow conditions at various temperatures. The proposed formulation incorporates temperature-dependent models for the SWRC (Vahedifard et al., 2018b) and effective stress (Vahedifard et al., 2019) to quantify the impact of temperature on apparent cohesion and, subsequently, on shear strength. The extended temperature-dependent SWRC and effective degree of saturation are then integrated into a steady infinite slope stability analysis of unsaturated soils. Results are compared against two sets of experimental results for sand reported in the literature.

2. Theory and formulations

The theoretical basis of the proposed slope stability framework is built upon the concept that, within the temperature range examined, the effect of temperature on the soil's shear strength can be primarily credited to thermal induced changes in apparent cohesion stemming from matric suction. The apparent cohesion represents the contribution of matric suction to the soil shear strength. Temperature dependency of apparent cohesion is captured by employing temperature-dependent models for the SWRC and effective stress, which are then used in an infinite slope stability analysis of unsaturated soils. The proposed formulation employs the suction stress-based effective stress approach (Lu and Likos, 2004, 2006; Lu et al., 2010), in which the shear strength criteria of unsaturated soils can be effectively defined using the classic shear strength parameters (c' and ϕ') and the SWRC (Lu et al., 2010). Thus, the backbone and theoretical basis of the proposed slope stability formulation is the recently developed temperature-dependent expressions for the SWRC (Vahedifard et al., 2018b) and effective stress (Vahedifard et al., 2019), two critical factors controlling the shear strength needed for slope stability analyses. Vahedifard et al. (2018b, 2019) extensively validated these temperature-dependent models for the SWRC and effective stress against several independent laboratory test results reported in the literature for different soil types. Interested readers are referred to Vahedifard et al. (2018b, 2019) for detailed derivation and validations results for the SWRC and effective stress models.

For simplicity, this study ignores the effect of thermally-induced vapor diffusion and only considers the variation of liquid water flow through Darcy's law. The thermally-induced water flow in soils can happen primarily due to the temperature effect on water retention properties, water resistance properties, suction gradients, and vapor diffusion (Philip and De Vries, 1957; Grant, 2003; Başer et al., 2018; Behbehani and McCartney, 2020). The analytical framework is derived considering drained heating and mechanical loading conditions. We did not consider the effects of thermal hysteresis and cracking in the proposed slope stability formulation. While this study focuses on the stability of bare intact slopes, temperature can affect the stability of unsaturated slopes through other factors including cracking and changes in vegetation (Jamalinia et al., 2019, 2020). Further, within the range of temperature examined, it is assumed that the thermal expansion will be negligible and has no notable effect on the soil shear strength.

2.1. Shear strength of unsaturated soil under elevated temperature

Based on Bishop's effective stress principle (Bishop, 1959), the suction stress-based effective stress of unsaturated soils is given as (Lu et al., 2010):

$$\sigma' = (\sigma - u_a - \sigma^s) \quad (1)$$

where σ is the total stress, u_a is the pore-air pressure, and σ^s is the suction stress, which can be defined as (Lu et al., 2010):

$$\sigma^s = -\psi S_e \tag{2}$$

where ψ is the matric suction and S_e represents the effective degree of saturation. Building on the suction stress based effective stress and the classic Mohr-Coulomb shear strength criteria, one can obtain the shear strength of unsaturated soils by:

$$\tau = c' + (\sigma - u_a - \sigma^s)tan\phi' \tag{3}$$

where τ is the shear strength, c' is the effective cohesion, ϕ' is the effective friction angle. The apparent cohesion quantifying the contribution of matric suction to shear strength can be determined as (Lu et al., 2010; Vahedifard et al., 2015):

$$c_{app} = -\sigma^s tan\phi' \tag{4}$$

where c_{app} is the apparent cohesion.

The above formulations (Eqs. 1 to 4), which were originally defined under ambient conditions, can be extended to elevated temperature conditions by employing temperature-dependent matric suction and the SWRC (Vahedifard et al., 2018b, 2019). The temperature dependency of matric suction can be expressed as (Grant and Salehzadeh, 1996):

$$\psi = \psi_{T_r}\left(\frac{\beta + T}{\beta_{T_r} + T_r}\right) \tag{5}$$

where T is temperature (in Kelvin), ψ_{Tr} is the matric suction at the reference temperature T_r. As defined, β_{Tr} is a regression parameter at the reference temperature, which depends on surface tension, enthalpy of immersion per unit area, and contact angle. The parameter β is calculated as (Grant and Salehzadeh, 1996):

$$\beta = \frac{-\Delta h\, T_r}{-\Delta h + a(cos\alpha)_{T_r} + b(cos\alpha)_{T_r} T_r} \tag{6}$$

where α is the temperature-dependent soil-water contact angle, a and b are fitting parameters that can be estimated as $a = 0.11766\ \mathrm{Nm^{-1}}$ and $b = -0.0001535\ \mathrm{Nm^{-1}K^{-1}}$ (Dorsey, 1940; Haar et al., 1984), and Δh is the enthalpy of immersion per unit area. The following equation is used to account for the temperature dependency of enthalpy of immersion per unit area (Watson, 1943):

$$\Delta h = \Delta h_{T_r}\left(\frac{1 - T_r}{1 - T}\right)^{0.38} \tag{7}$$

where Δh_{Tr} is the enthalpy of immersion per unit area at the reference temperature.

The temperature-dependent soil-water contact angle is given by (Grant and Salehzadeh, 1996):

$$cos\alpha = \frac{-\Delta h + TC_1}{a + bT} \tag{8}$$

where C_1 is a constant, which can be determined as (Grant and Salehzadeh, 1996):

$$C_1 = \frac{\Delta h_{T_r} + a(cos\alpha)_{T_r} + b(cos\alpha)_{T_r} T_r}{T_r} \tag{9}$$

Vahedifard et al. (2018b) used the aforementioned temperature-dependent equations for matric suction and enthalpy of immersion to extend the SWRC models of Brooks and Corey (1964) (referred to as the BC model) to temperature-dependent conditions as follows:

Table 1
Hydraulic, thermal and mechanical parameters of hypothetical soils used in the parametric study.

Soil	Hydraulic*				Thermal**			Mechanical***	
	n	β' (kPa)	Δh_{T_r} (J/m^2)	k_{in} (m/s)	λ_{dry} (W/(mK))	λ_{sat} (W/(mK))	S_f	ϕ' (deg.)	c' (kPa)
Clay	2	33.33	−0.516	4.5E-15	0.239	1.556	0.171	25	10
Silt	3	3.33	−0.516	1E-14	0.198	1.216	0.246	30	2
Sand	4	3	−0.285	1E-12	0.256	2.185	0.064	35	0

* data from Lu and Likos (2004) and Grant and Salehzadeh (1996).
** data from Lu and Dong (2015).
*** data from Lu and Godt (2008) and Chowdhury and Azam (2016).

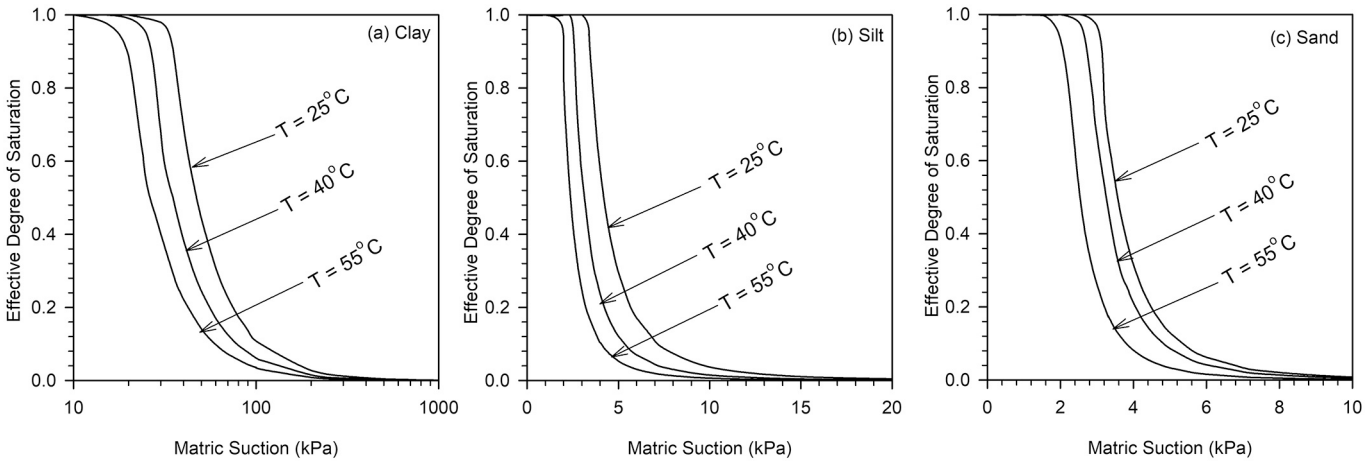

Fig. 1. Effective degree of saturation versus matric suction for hypothetical soils at different temperatures: (a) clay; (b) silt; and (c) sand.

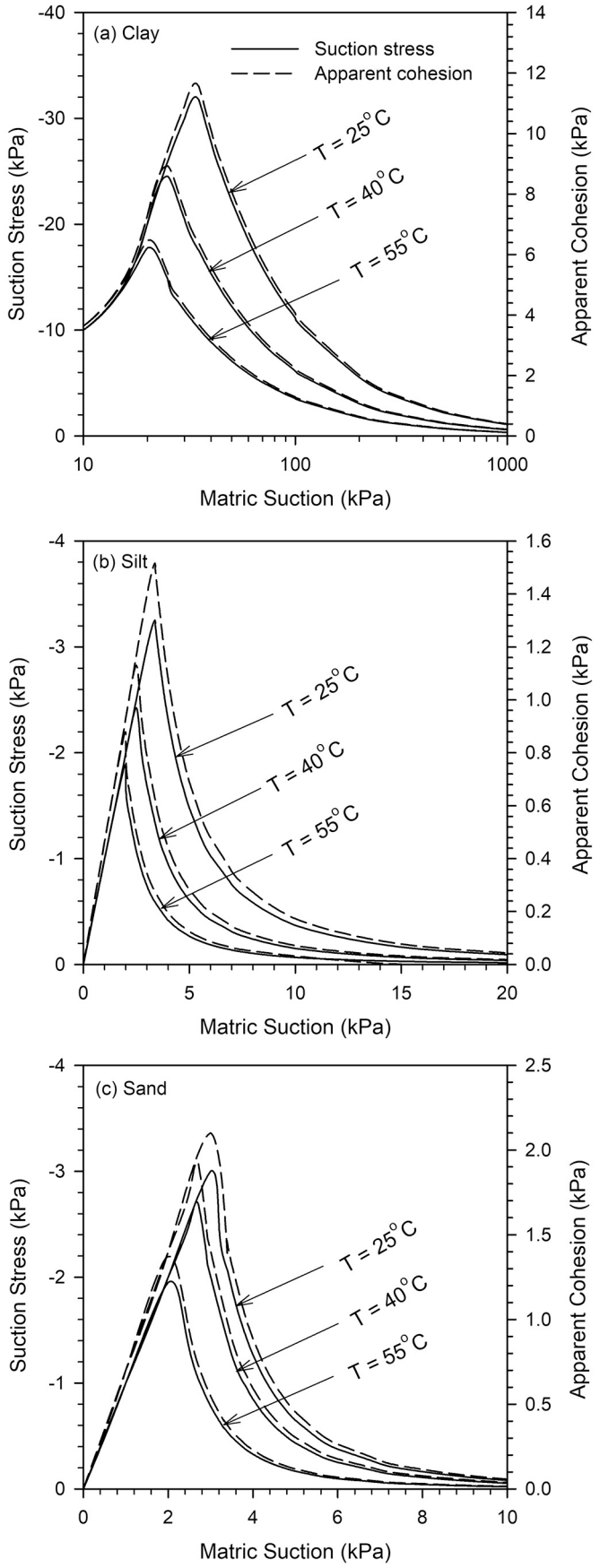

Fig. 2. Suction stress and apparent cohesion versus matric suction for hypothetical soils at different temperatures: (a) clay; (b) silt; and (c) sand.

$$S_e = \left(\frac{\beta'}{\psi\left(\frac{\beta_{T_r}+T_r}{\beta+T}\right)} \right)^n \tag{10}$$

where β' is a fitting parameter related to the air-entry suction (kPa), n is a fitting parameter representing the pore-size distribution. The effect of hydraulic hysteresis (on main wetting and drying paths) can be considered by adjusting the SWRC fitting parameters in Eq. 10. One can obtain the SWRC fitting parameters for the drying path using laboratory-measured data and then, use empirical correlations to estimate the wetting SWRC parameters (Likos et al., 2014). By substituting Eqs. 5 and 10 into Eq. 2 and Eq. 4, the temperature-dependent suction stress characteristic curve (SSCC) and apparent cohesion, respectively, can be written as:

$$\sigma^s = -\left(\frac{\beta'}{\psi\left(\frac{\beta_{T_r}+T_r}{\beta+T}\right)} \right)^n \psi\left(\frac{\beta_{T_r}+T_r}{\beta+T}\right) \tag{11}$$

$$c_{app} = tan\phi' \left(\frac{\beta'}{\psi\left(\frac{\beta_{T_r}+T_r}{\beta+T}\right)} \right)^n \psi\left(\frac{\beta_{T_r}+T_r}{\beta+T}\right) \tag{12}$$

To illustrate the effect of temperature, a parametric study is performed for hypothetical clay, silt, and sand. Table 1 shows the hydraulic parameters used to plot SWCC, SSCC, and apparent cohesion for each of the hypothetical soils at different temperatures. The data are obtained from similar soils reported by Lu and Likos (2004) for n and β' and by Grant and Salehzadeh (1996) for Δh_{T_r}.

Fig. 1 shows the relationship between effective degree of saturation and matric suction for different soils at temperatures of 25, 40, and 55 °C. The results confirm that increasing temperature can cause a downward shift in the SWRCs. This is because of thermal induced changes in surface tension, contact angle, and enthalpy of immersion (e.g., Grant and Salehzadeh, 1996; Roshani and Sedano, 2016; Vahedifard et al., 2018b).

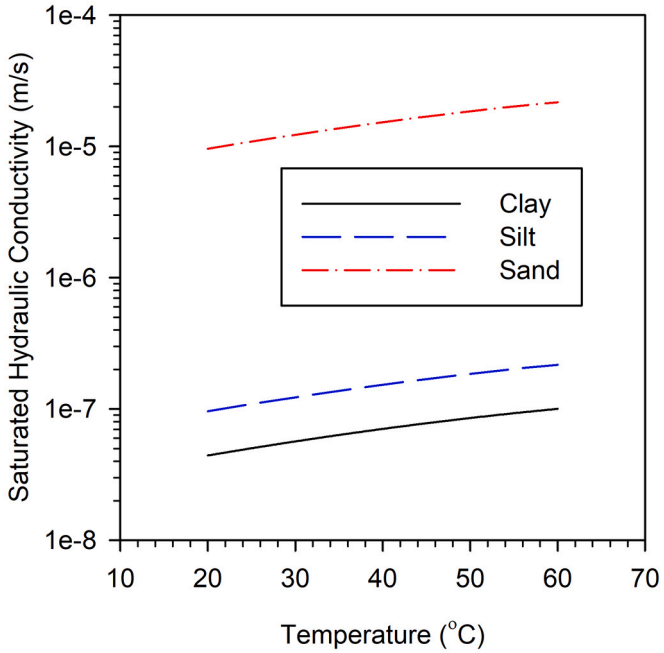

Fig. 3. Variation of saturated hydraulic conductivity with temperature for clay, silt, and sand.

Fig. 2 depicts changes in suction stress (the left y-axis) and apparent cohesion (the right y-axis) with matric suction at temperatures of 25, 40, and 55 °C. For all soils and at a given temperature, suction stress and apparent cohesion exhibit a non-monotonic trend versus different matric suction. The trends of both suction stress and apparent cohesion are affected by temperature-induced changes in matric suction and effective degree of saturation. Since the apparent cohesion is merely a function of suction stress and the angle of friction, the physical phenomena involved for both suction stress and apparent cohesion is the same as the friction angle is kept constant. Three distinct mechanisms can be noted. Firstly, at low matric suctions, suction stress (or apparent cohesion) is almost the same for different temperatures. Secondly, the peak of suction stress (absolute value) decreases at elevated temperatures. Lastly, for relatively high matric suctions, the absolute value of suction stress decreases with an increase in temperature. The distinct behavior of suction stress for various temperature and matric suction ranges may arise from differences in the dominating water retention mechanism at each range of matric suction (Vahedifard et al., 2019).

2.2. Temperature-dependent shear strength profiles versus depth under steady flow

The matric suction typically varies within a slope depending on surface flux boundary conditions, location of water table, slope configuration, and soil type. Using Darcy's law, Lu and Griffiths (2004) developed an analytical solution for steady-state suction stress profiles versus depth in terms of seepage condition and hydraulic parameters. The Lu and Griffiths (2004) formulation is extensively used for slope stability analysis purposes using different mechanisms such as the infinite (Lu and Godt, 2008) or logspiral (Vahedifard et al., 2016b) failure mechanisms. In this study, we extended the Lu and Griffiths (2004) formulation to account for the effect of temperature by employing the temperature-dependent expression for suction stress presented in the previous section. The temperature-dependent suction stress profile versus depth will be then used to derive depth profiles for temperature-dependent shear strength and the FOS under steady flow.

We derived the following temperature-dependent expression for matric suction profile versus depth under one-dimensional steady flow (see detailed derivation in Appendix I):

$$\psi = \frac{\gamma_w}{\beta'} ln\left[\left(1+\frac{q}{k_s}\right)e^{-\beta' z} - \frac{q}{k_s}\right]\left(\frac{\beta_{T_r}+T_r}{\beta+T}\right) \tag{13}$$

where q is the steady vertical fluid flow rate (negative for infiltration and positive for evaporation), γ_w is the unit weight of water, $k_s$is the saturated hydraulic conductivity, which can be affected by temperature because of the effect of temperature on water viscosity (Pillsbury, 1950; Philip, 1969). The temperature dependency of the saturated hydraulic conductivity can be described by (Constantz, 1982):

$$k_s = \frac{k_{in}\rho_w g}{\eta(T)} \tag{14}$$

where k_{in} is the intrinsic hydraulic conductivity assumed to be dependent only on the soil type, ρ_w is the density of water, g is the gravitational acceleration, and $\eta(T)$ is the water viscosity as a function of temperature as (Lide, 1995):

$$\eta(T) = 0.0002601 + 0.001517exp[-0.034688\times(T-273)] \tag{15}$$

Fig. 3 shows the change in the saturated hydraulic conductivity with temperature for clay, silt, and sand. In these plots, the porosity is assumed to be constant at all temperatures. It is observed that the saturated hydraulic conductivity increases with an increase in temperature. One of the reasons for this variation could be due to reduction in the water viscosity under elevated temperatures (Constantz, 1982; Cui et al., 2008).

Using the BC SWRC model and Gardner (1958)'s hydraulic conductivity function, the temperature-dependent model for effective degree of saturation depth profile is written as (see derivation in Appendix I):

$$S_e = \left\{exp\left[ln\left(\left(1+q/k_s\right)e^{-\beta' z} - q/k_s\right)\left(\frac{\beta_{T_r}+T_r}{\beta+T}\right)\right]\right\}^{1/n} \tag{16}$$

By substituting Eqs. 13 and 16 into Eq. 2 and Eq. 4, the final equations for temperature-dependent suction stress and apparent cohesion profiles, respectively, are:

$$\sigma^s = -exp\left\{ln\left[\left(1+\frac{q}{k_s}\right)e^{-\beta' z} - \frac{q}{k_s}\right]\left(\frac{\beta_{T_r}+T_r}{\beta+T}\right)\right\}^{1/n} \frac{\gamma_w}{\beta'} ln\left[\left(1+\frac{q}{k_s}\right)e^{-\beta' z} - \frac{q}{k_s}\right]\left(\frac{\beta_{T_r}+T_r}{\beta+T}\right) \tag{17}$$

$$c_{app} = tan\phi' exp\left\{ln\left[\left(1+\frac{q}{k_s}\right)e^{-\beta' z} - \frac{q}{k_s}\right]\left(\frac{\beta_{T_r}+T_r}{\beta+T}\right)\right\}^{1/n} \frac{\gamma_w}{\beta'} ln\left[\left(1+\frac{q}{k_s}\right)e^{-\beta' z} - \frac{q}{k_s}\right]\left(\frac{\beta_{T_r}+T_r}{\beta+T}\right) \tag{18}$$

Similarly, the temperature-dependent depth profile for effective stress of unsaturated soils is given by:

$$\sigma' = (\sigma - u_a) + exp\left\{ln\left[\left(1+\frac{q}{k_s}\right)e^{-\beta' z} - \frac{q}{k_s}\right]\left(\frac{\beta_{T_r}+T_r}{\beta+T}\right)\right\}^{1/n} \frac{\gamma_w}{\beta'} ln\left[\left(1+\frac{q}{k_s}\right)e^{-\beta' z} - \frac{q}{k_s}\right]\left(\frac{\beta_{T_r}+T_r}{\beta+T}\right) \tag{19}$$

From Eqs. 3 and 19, the shear strength profiles of unsaturated soils under elevated temperature is evaluated by:

$$\tau = c' + \left(\begin{array}{c} (\sigma - u_a) + exp\left\{ ln\left[\left(1 + \frac{q}{k_s}\right) e^{-\beta' z} - \frac{q}{k_s} \right] \left(\frac{\beta_{T_r} + T_r}{\beta + T} \right) \right\}^{1/n} \\ \frac{\gamma_w}{\beta'} ln\left[\left(1 + \frac{q}{k_s}\right) e^{-\beta' z} - \frac{q}{k_s} \right] \left(\frac{\beta_{T_r} + T_r}{\beta + T} \right) \end{array} \right) tan\phi' \tag{20}$$

2.3. Temperature-dependent factor of safety under steady seepage

The FOS of infinite slopes is generally calculated as the ratio of shear strength to the shear stress of soil (Duncan and Wright, 2005). For unsaturated conditions, the FOS can be determined by integrating the suction stress concept into the well-known equation for infinite slope stability (Lu and Godt, 2008):

$$FOS = \frac{tan\phi'}{tan\delta} + \frac{2c'}{\gamma H_{ss} sin2\delta} - \frac{\sigma^s (tan\delta + cot\delta) tan\phi'}{\gamma H_{ss}} \tag{21}$$

where δ is the angle of slope, γ is the unit weight of soil, $H_{ss} = (H_{wt} - z)$ is the height of the sliding surface, with H_{wt} being the total height between the water table and the ground surface, and z is the distance from the water table towards the ground surface. In the case of near-surface problems, the pore-air pressure can be reasonably assumed to be constant and equivalent to atmospheric pressure (Lu and Godt, 2008; Godt et al., 2012). Fig. 4 depicts the geometry and different variables. It is assumed that the unit weight of soil is constant.

The primary focus of the study is to quantify the impact of temperature on the stability of unsaturated slopes. Thus, the effects of steady seepage are considered on the soil above the water table. In such scenarios, the failure surface is considered to be well above the water table and so, there is no need to incorporate the effects of seepage parallel to the slope in the soil below the water table in the derivation. That is, the seepage below the water table has no effect on the strength and shear stress acting along the failure plane. Failure above the saturated zone implies some variation in strength with depth. In field conditions, several slope failures, specifically shallow rainfall-triggered landslides, have been reported where the slope failed while still in an unsaturated state and the failure plane is within the unsaturated zone (e.g., Duncan and Wright, 2005; Godt et al., 2012; Montgomery and Dietrich, 1994; Godt et al., 2009). The same assumptions (i.e., ignoring the seepage parallel to the slope in the soil below the water table, and the failure surface above the water table) have been extensively adopted in slope stability analyses of unsaturated slopes (e.g., Godt et al., 2012; Montgomery and Dietrich, 1994; Godt et al., 2009).

Substituting the suction stress formulation that is extended through the BC model (Eq. 17) into Eq. 21, the FOS at elevated temperatures is calculated as:

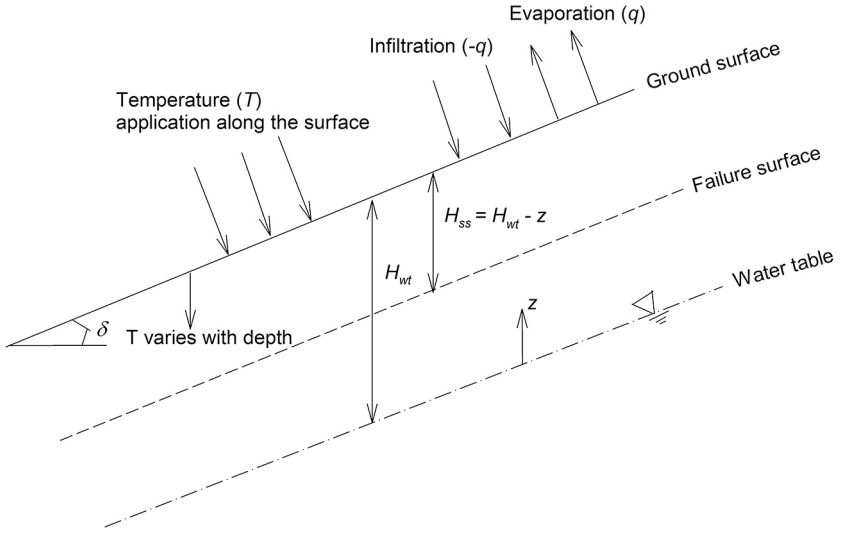

Fig. 4. Diagram of infinite slope stability for unsaturated soils under temperature-dependent and seepage conditions.

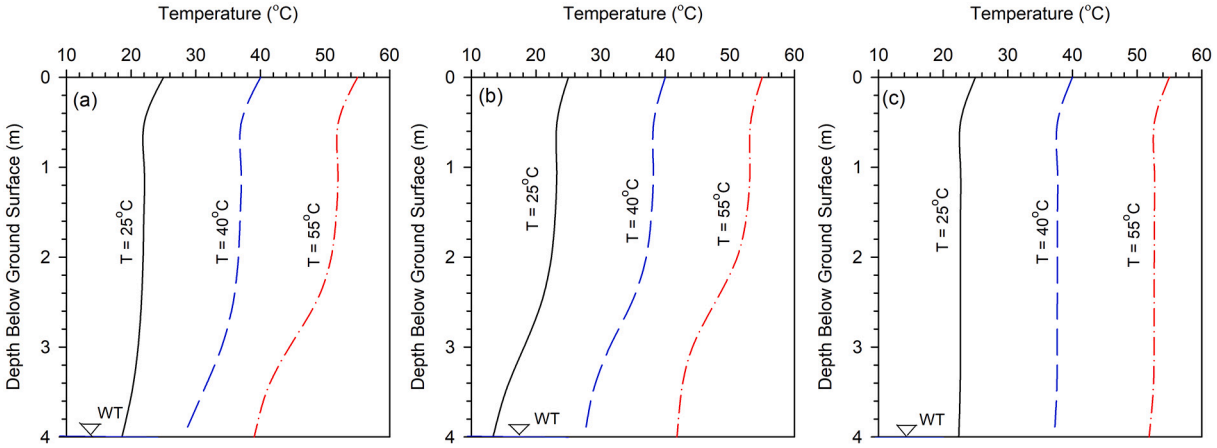

Fig. 5. Variation of temperatures with depth for a constant heat flux density of 3 Wm^{-2}: a) sand, b) silt, and c) clay for surface temperatures of 25 °C, 40 °C, and 55 °C.

$$FOS = \frac{tan\phi'}{tan\delta} + \frac{2c'}{\gamma(H_{wt}-z)sin2\delta} + exp\left\{ ln\left[\left(1+\frac{q}{k_s}\right)e^{-\beta' z} - \frac{q}{k_s}\right]\left(\frac{\beta_{T_r}+T_r}{\beta+T}\right)\right\}^{1/n} \times \frac{\gamma_w}{\beta'} ln\left[\left(1+\frac{q}{k_s}\right)e^{-\beta' z} - \frac{q}{k_s}\right] \frac{\left(\frac{\beta_{T_r}+T_r}{\beta+T}\right)(tan\delta + cot\delta)tan\phi'(z)}{\gamma(H_{wt}-z)} \quad (22)$$

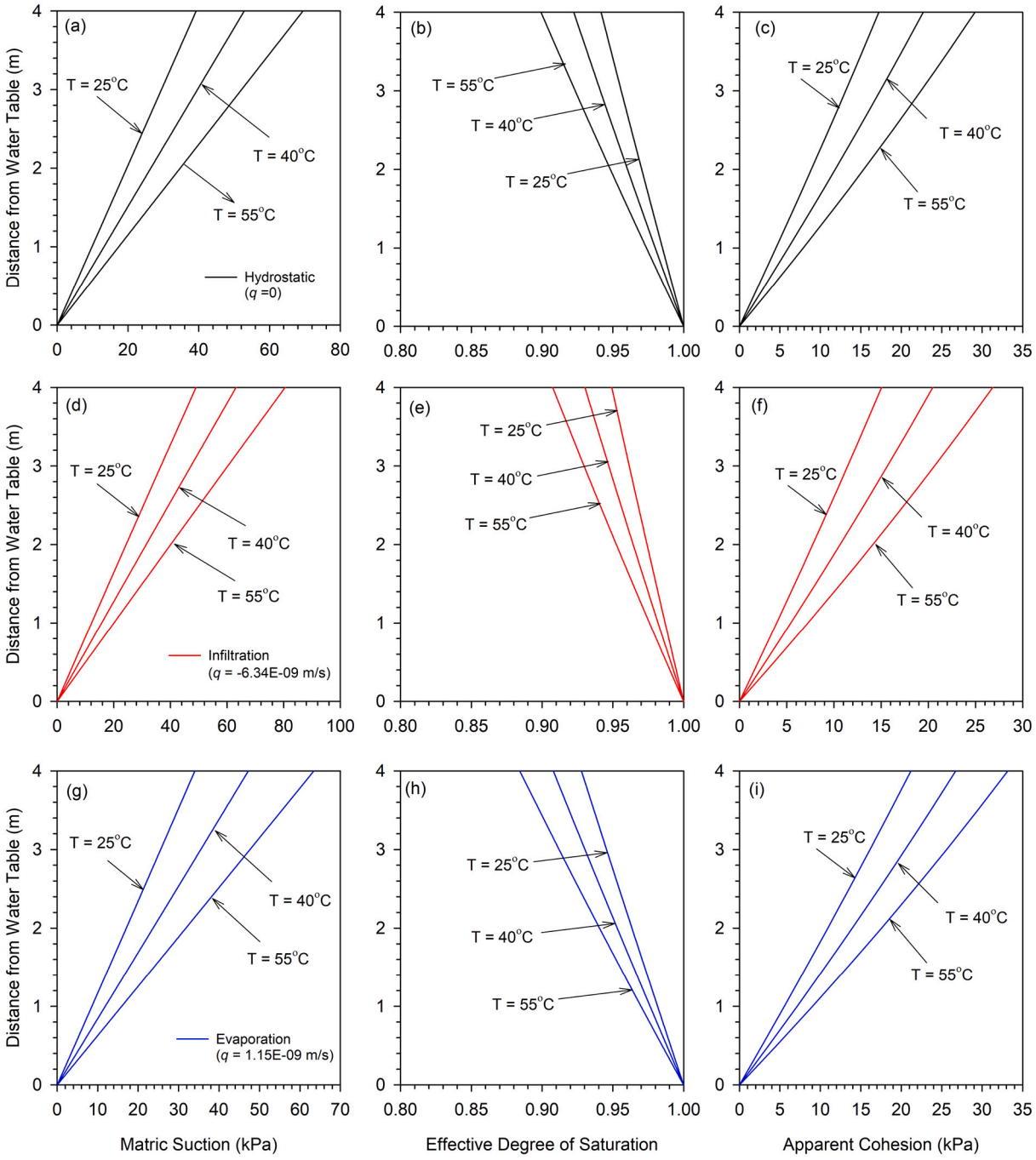

Fig. 6. Depth profile of matric suction, effective degree of saturation and apparent cohesion for: (a-c) hydrostatic condition; (d-f) infiltration condition; and (g-i) evaporation condition, for the clayey slope with $\delta = 30°$ at temperatures 25, 40 and 55 °C.

The soil temperature gradient versus depth can be defined using Fourier's law as:

$$\frac{dT}{dz} = -\frac{q_h}{\lambda} \tag{23}$$

where q_h is the heat flux density (Wm^{-2}), which depends on the type of material and net radiation and λ is the thermal conductivity (W/mK) that can be linked to the degree of saturation using a thermal conductivity function (TCF) as (Lu and Dong, 2015):

$$\frac{\lambda - \lambda_{dry}}{\lambda_{sat} - \lambda_{dry}} = 1 - \left(1 + \left(\frac{S}{S_f}\right)^m\right)^{1/m-1} \tag{24}$$

where λ_{sat} and λ_{dry} are thermal conductivities at saturated (maximum) and dry (minimum) states, respectively, S_f is the degree of saturation at which the funicular regime of water retention starts, and m is fitting parameter representing the pore fluid network connectivity, which is related to the pore-size parameter in SWRC models (Lu and Dong, 2015). In this study, we take m to be equal to BC SWRC's n parameter. Obtained from the data reported in Lu and Dong (2015), Table 1 shows the parameters used to calculate thermal conductivity for different soils.

The depth profiles of temperature can be determined using the concepts of thermal conductivity and Fourier's law. Fig. 5 shows the temperature gradient for sand, silt, and clay soils for three surface temperatures of 25, 40, and 55 °C, respectively. The temperature profiles versus depth are calculated by assuming a constant heat flux and

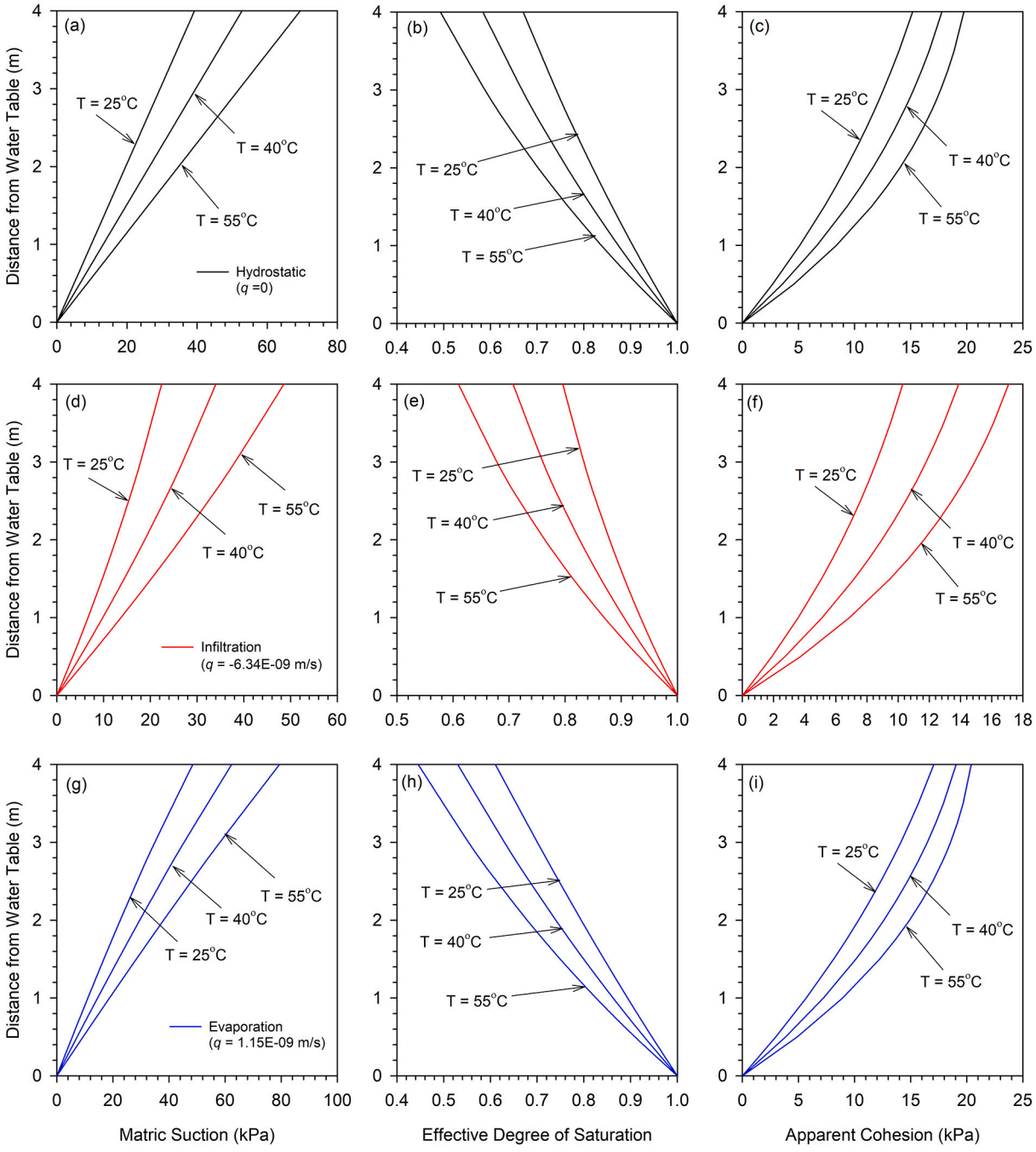

Fig. 7. Depth profile of matric suction, effective degree of saturation and apparent cohesion for: (a-c) hydrostatic condition; (d-f) infiltration condition; and (g-i) evaporation condition, for the silty slope with $\delta = 30^\circ$ at temperatures 25, 40 and 55 °C.

hydrostatic (q = 0) conditions. Assuming a constant heat flux density of 3 Wm^{-2}, a similar decreasing trend of temperature with depth is noted for all three soils. This is attributed to the increase in thermal conductivity as the soil's saturation level increases towards the water table.

3. Parametric study and discussion

In this section, the effects of temperature on matric suction (Eq. 13), effective degree of saturation (Eq. 16), apparent cohesion (Eq. 18), shear strength (Eq. 20), and FOS (Eq. 22) for the three hypothetical soils are investigated under different flow conditions. The input parameters are shown in Table 1. All calculations are performed for the water table depth of H_{wt} = 4 m, and the unit weight of the soil of γ = 21 kN/m^3. Slope angles (δ) of 30, 30 and 35° are used for the clayey, silty, and sandy slopes, respectively. For each soil, three different flow rates are examined: infiltration ($q = -6.34 \times 10^{-9}$ m/s), hydrostatic (no flow, q = 0), and evaporation ($q = 1.15 \times 10^{-8}$ m/s). These flow rates are similar to those used in the literature for parametric study purposes (Lu and Godt, 2008; Vahedifard et al., 2015).

Fig. 6 demonstrates the depth profiles for matric suction (Fig. 6a, d, and g), effective degree of saturation (Fig. 6b, e, and h), and apparent cohesion (Fig. 6c, f, and i) of the clayey soil under steady flow conditions at surface temperatures of 25, 40, and 55 °C. The results of each property are presented for different flow conditions through three rows:

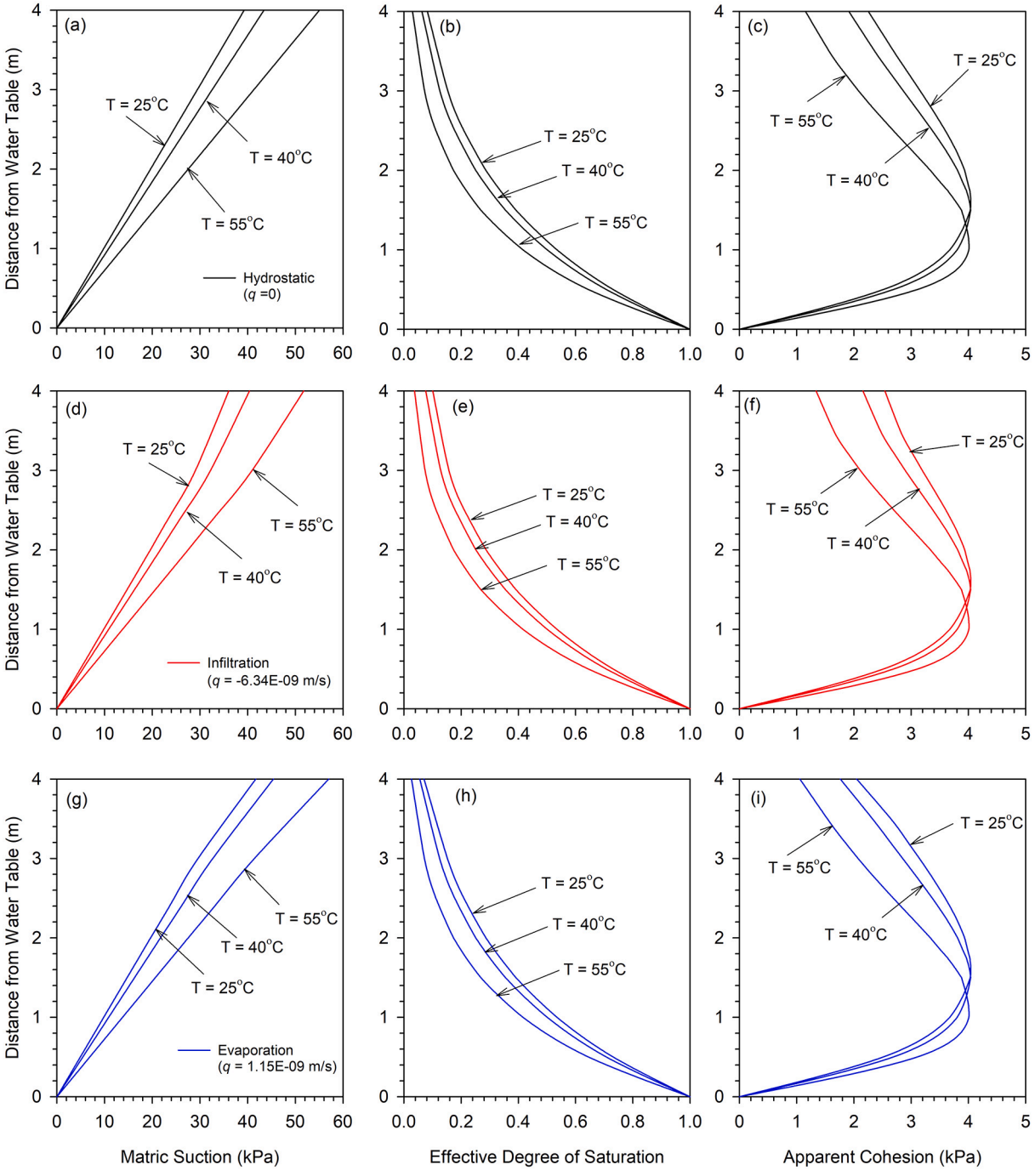

Fig. 8. Depth profile of matric suction, effective degree of saturation and apparent cohesion for: (a-c) hydrostatic condition; (d-f) infiltration condition; and (g-i) evaporation condition, for the sandy slope with δ = 35° at temperatures 25, 40 and 55 °C.

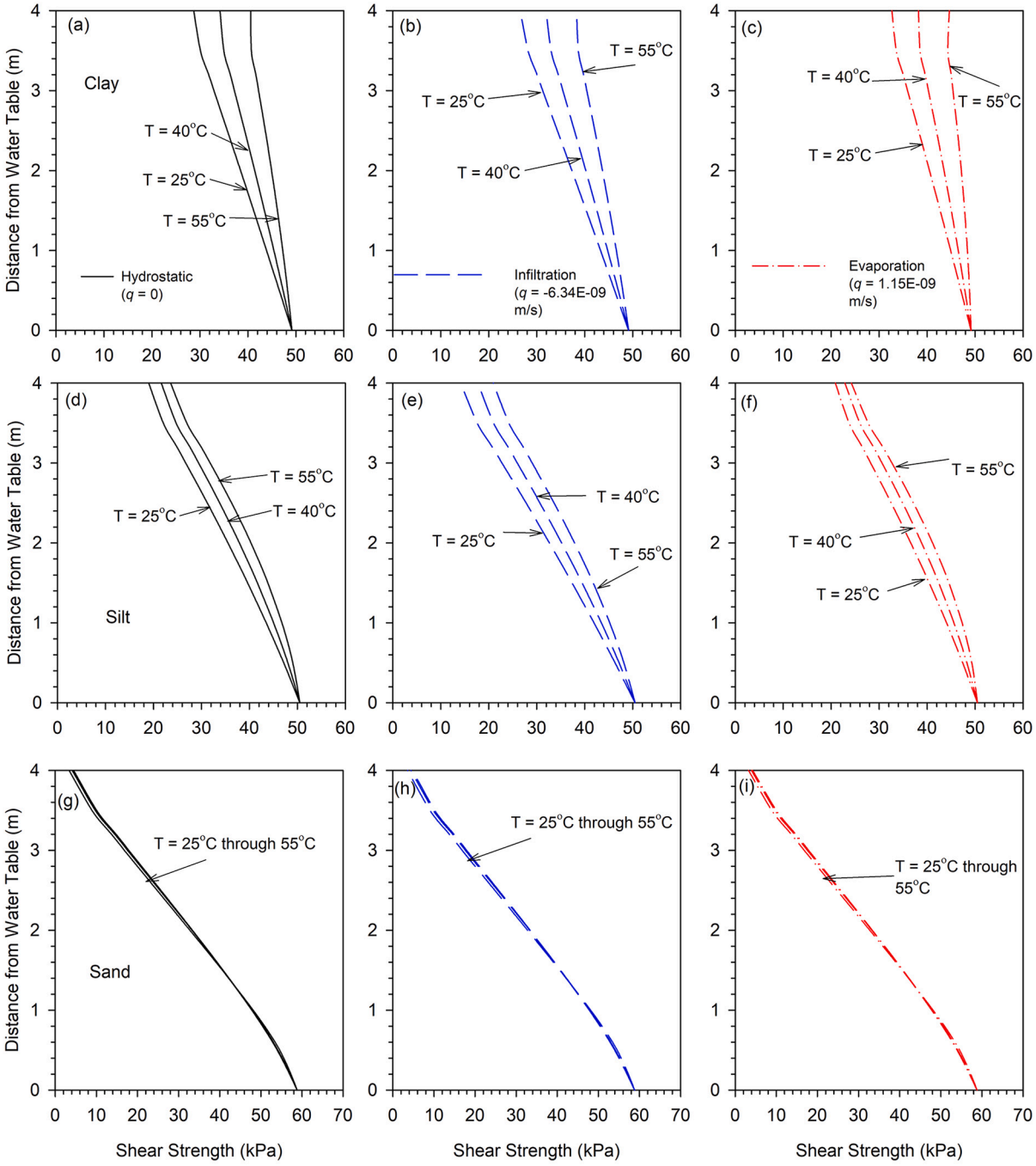

Fig. 9. Depth profiles of shear strength for hydrostatic, infiltration and evaporation conditions of (a-c) clay, (d-f) silt and (g-i) sand soils at temperatures $T = 25$ °C, 40 °C, and 55 °C.

hydrostatic (Fig. 6a, b, and c), infiltration (Fig. 6d, e, and f), and evaporation (Fig. 6g, h, and i) conditions. As shown, the profiles of each property are sensitive to the flow conditions and elevated temperatures. For example, at $T = 25$ °C, the curve shifts to the left of hydrostatic for the infiltration condition and right of hydrostatic for the evaporation condition. For the given flow rate, the matric suction and apparent cohesion shift to the right, and the effective degree of saturation moves to the left as temperature increases. A similar monotonic trend is seen for all variables at different temperatures.

For all flow conditions and depths, Fig. 6a shows that the matric suction increases with an increase in temperature at a given depth. The percentage increase in the matric suction is relatively higher at the ground surface since the temperature is maximum and the degree of saturation is minimum. On the other hand, as seen in Fig. 6b, the effective degree of saturation decreases with an increase in temperature. Similarly, a greater variation is observed close to the surface than the near water table. At a given depth, the trend of predicted changes in matric suction and effective degree of saturation with temperature is consistent with the experimental data (Grant and Salehzadeh, 1996; She and Sleep, 1998).

As shown in Fig. 6c, the apparent cohesion increases as temperature increases, this is due to the temperature-induced increase in matric suction, and the temperature-induced decrease in the effective degree of saturation. At a depth of 2 m, the apparent cohesion increases by approximately 33% and 73% for hydrostatic, increases by 37% and 80% for infiltration, and increases by 28% and 60% for evaporation

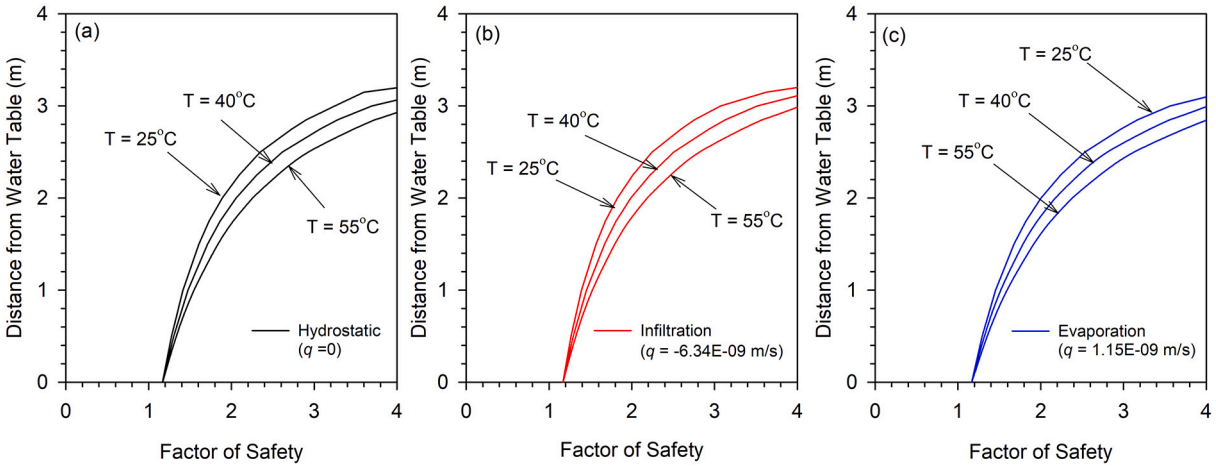

Fig. 10. Depth profile of factor of safety at (a) hydrostatic condition; (b) infiltration condition; and (c) evaporation condition, for the clayey slope with $\delta = 30^{\circ}$ at temperatures 25, 40 and 55 °C.

conditions by increasing temperature from 25 °C to 40 °C and 60 °C, respectively. The apparent cohesion of clayey soils, in general, primarily depends on physicochemical forces like van der Waals attractions and electrostatic forces near the contacts of soil particles (Lu and Likos, 2006). Under elevated temperatures, the negative pore-water pressures decrease due to the reduction in degree of saturation and change in physicochemical forces, therefore increasing the interparticle forces (Plum and Esrig, 1969).

Fig. 7 depicts the depth profiles for matric suction (Fig. 7a, d, and g), effective degree of saturation (Fig. 7b, e, and h) and shear strength (Fig. 7c, f, and i) for the silty soil under different flow conditions at temperatures of 25, 40, and 55 °C. The trends are similar to those seen for the clayey soil. The relative change in each property might be different; however, the underlying physics dominating the observed trends remains the same. The apparent cohesion increases by 26% and 52% (for hydrostatic), 40% and 80% (for infiltration), 22% and 44% (for evaporation) by increasing temperature from 25 °C to 40 °C and 60 °C.

Fig. 8 shows the results for the sandy soil. The matric suction (Fig. 8a, d, and g) increases and the effective degree of saturation (Fig. 8b, e, and h) decreases with an increase in temperature for all flow conditions. Unlike the clay and silt soils, the trend of apparent cohesion (Fig. 8c, f, and i) with temperature is non-monotonic. The non-monotonic behavior of sand under ambient conditions is in accordance with the data reported in the literature (Lu and Likos, 2006; Lu and Godt, 2008). The apparent cohesion increases minimally close to the water table (up to 1 m above the water table) and decreases towards the surface by increasing temperature from 25 °C to 40 °C and 55 °C. For example, under various flow conditions, for instance at 0.5 m from the water table, the apparent cohesion increases by 7% and 24% by increasing the temperatures from 25 °C to 40 °C, and 55 °C. The apparent cohesion near the ground surface, for instance at 3 m from the water table (or 1 m below the surface) decreases by 9% and 34% by increasing the temperatures from 25 °C to 40 °C, and 55 °C for various flow conditions.

Fig. 9 shows the depth profiles of shear strength with respect to different soils, temperatures, and flow conditions. Consistent with the trends seen for apparent cohesion in Figs. 6 to 8, it is seen in Fig. 9 that the trend of shear strength for clay and silt is monotonic and noticeable but for sand is non-monotonic and insignificant. The trend of shear strength is completely dependent and similar to the variation of suction stress with temperature, as the friction angle is assumed to be unchanged with a range of temperatures considered. The shear strength variation with depth under both ambient and elevated temperatures can be significant in the case of fine-grained soils (clay and silt). However, due to the lack of physiochemical forces, the change is not notable for coarse-grained soils such as sand. For clay and silt under various flow conditions, the shear strength increases with an increase in temperature. For sand, the shear strength increases close to the water table and then decreases towards the ground surface when the temperature is increased from 25 °C to 40 °C and 55 °C.

Fig. 10 shows the changes in FOS at different temperatures and flow

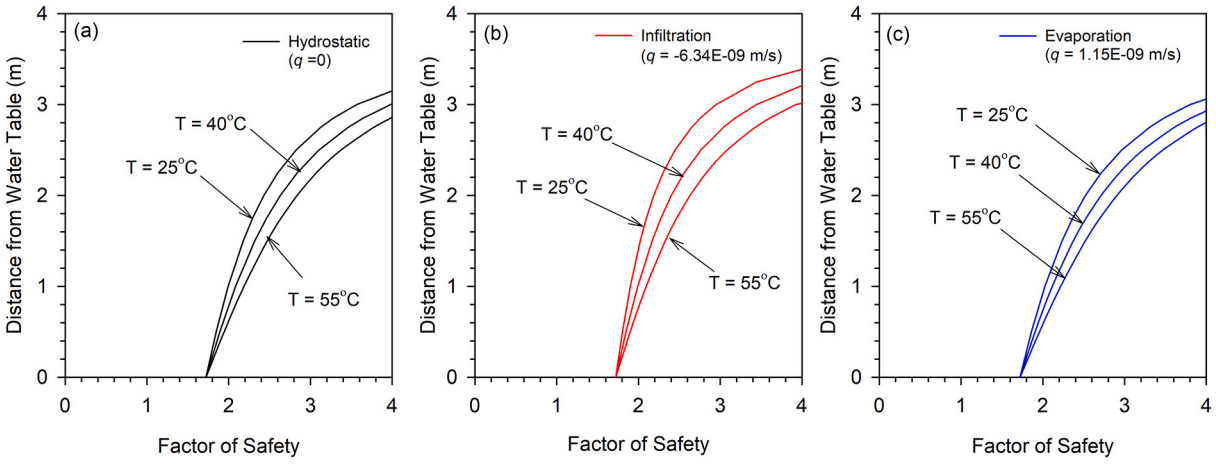

Fig. 11. Depth profile of factor of safety at (a) hydrostatic condition; (b) infiltration condition; and (c) evaporation condition, for silty slope with $\delta = 30^{\circ}$ at temperatures 25, 40 and 55 °C.

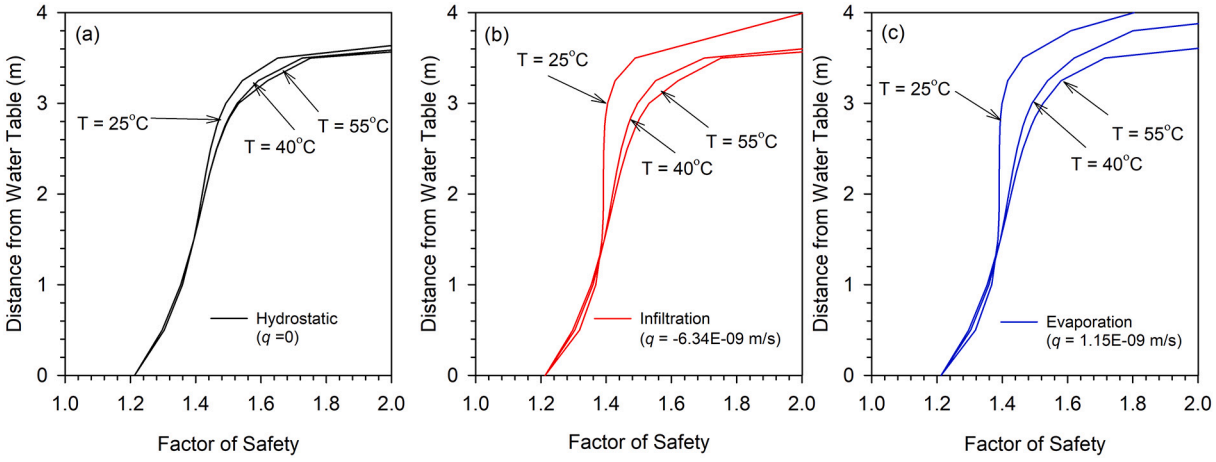

Fig. 12. Depth profile of factor of safety at (a) hydrostatic condition; (b) infiltration condition; and (c) evaporation condition for the sandy slope with $\delta = 35°$ at temperatures 25, 40 and 55 °C.

conditions for the clayey soil slope. Fig. 10a, b, and c present the changes in temperature dependent FOS at hydrostatic, infiltration and evaporation conditions, respectively. As observed in the shear strength results, the increase in the magnitude of shear strength causes the FOS of clay slope to increase at elevated temperatures. The impact of temperature on the FOS increases as the distance from the water table increases. This behavior results because the degree of saturation decreases towards the ground surface.

Fig. 11 shows the FOS of the silty slope at different temperatures and flow conditions. Similar to the clay soil slope, the results indicate an increasing trend of the FOS at elevated temperatures under all flow conditions for the silty soil slope. As temperature increases, the FOS increases throughout the profile. The thermally induced change in the FOS is the greatest near the ground surface and decreases near the water table.

Fig. 12 shows the depth profiles for the FOS of the sandy soil slope at elevated temperatures. The results indicate a non-monotonic trend of the FOS at elevated temperatures under all flow conditions. With an increase in temperature, as shown, the FOS increases slightly near the water table and then decreases as the distance from the water table increases. The changes in FOS due to elevated temperatures for the sand slope is small compared to the two finer-grained soil slopes.

To further illustrate the temperature effect on the FOS, the variation of the FOS versus temperature for clay, silt, and sand under different flow conditions are shown in Fig. 13. As seen, for all soils, the rate of change in the FOS with increasing temperature is higher near the ground surface and the rate reduces when approaching the water table. Fig. 13a demonstrates the changes in the FOS at 2 m above the water table (i.e., 2 m below the ground surface) and 3 m above the water table (i.e., 1 m below the ground surface) for the clay soil. At 3 m above the water table, the FOS increases by approximately 14% and 30% by increasing the surface temperature from 25 °C to 40 °C and 55 °C under the hydrostatic condition. For the infiltration and evaporation conditions, the FOS of the clay slope increases by approximately 14%, 31% and 13%, 28%, respectively, by increasing the surface temperature from 25 °C to 40 °C and 55 °C. Closer to the water table (i.e., 2 m), the FOS of the clay slope increases by approximately 9% and 19% under the hydrostatic condition, increases by approximately 9%, 20% and 9%, 19% for infiltration and evaporation conditions, respectively, by increasing the temperature from 25 °C to 40 °C and 55 °C.

For the silt slope, as shown in Fig. 13b, at a distance of 3 m from the water table the FOS increases by approximately 12%, and 22% by increasing the temperature from 25 °C to 40 °C and 55 °C under the hydrostatic condition. With the infiltration and evaporation conditions, the FOS increases by approximately 17%, 33% and 10%, 18%, respectively. At 2 m distance above the water table, the FOS increases by approximately 8% and 17% for the hydrostatic condition and by approximately 10%, 20% and 8%, 15% for the infiltration and evaporation conditions, respectively. For the sand soil (Fig. 13c), at a depth 1 m above the water table, the FOS increases approximately by 0.5%, 1% and at 3 m depth, it decreases by approximately 2%, 8% by increasing temperature from 25 °C to 40 °C, and 55 °C, respectively, under all

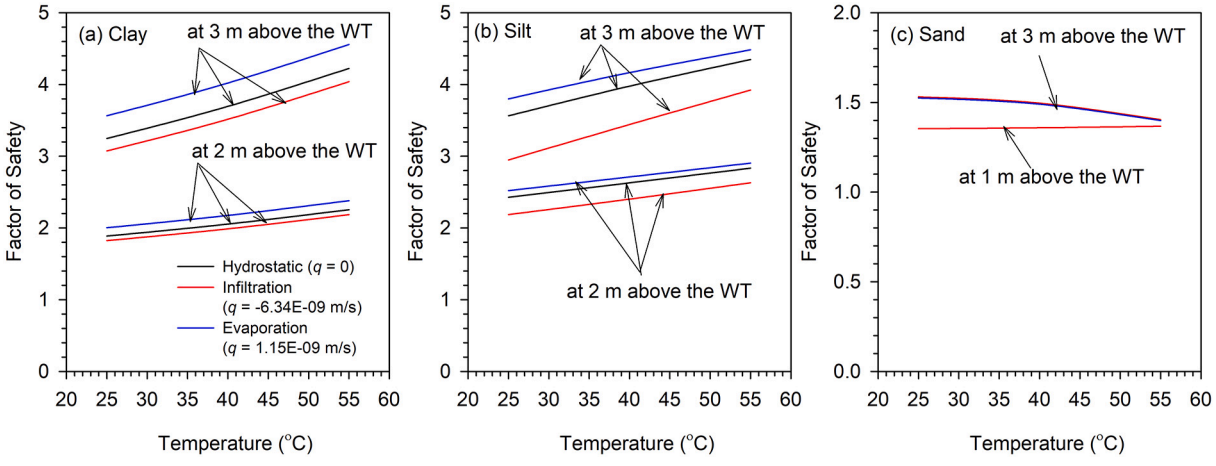

Fig. 13. Factor of safety versus temperature for (a) clay; (b) silt; and (c) sand.

seepage conditions. The effect of temperature on the capillary mechanism is the main factor that contributes to the observed trend in the sandy soil. For the sandy slope, overall, the flow and thermal conditions are shown to have a negligible effect.

4. Validation

We used two sets of experimental results reported by Wilson (1990) and Song et al. (2014) to test the validity of the proposed formulations. Because our derivation is developed for a steady-state flow condition, we used the measured effective degree of saturation, temperature, suction (where available) reported by these references at the initial state in which the measured data were collected under steady-state conditions. It is noted the FOS calculations are not directly validated since we could not find any study in the literature presenting the FOS for unsaturated soils at different temperatures. Nevertheless, the effective degree of saturation and matric suction are the key factors controlling the shear strength needed for slope stability analyses. While the presented model can certainly benefit from further validation against more laboratory and field measured data for different soils, we believe the level of validation presented suffices to prove the validity of the presented formulation.

Wilson (1990) conducted drying tests on Beaver Creek sand columns in a climatically controlled environmental chamber. An evaporation pan, thermocouples, and scales were utilized to measure evaporative fluxes, temperature, and water content in the columns at different intervals of time, respectively. Fig. 14a shows the predicted and measured values for the SWRC for Beaver creek sand. With the parameters shown in Fig. 14a, a very good prediction can be obtained from the temperature-dependent BC SWRC model. Using the hydraulic properties of Beaver creek sand, the fitted SWRC parameters (see Fig. 14a), temperature profiles (see Fig. 14b), evaporative fluxes (see Fig. 14c), and the saturated hydraulic conductivity of k_s = 8.4E-06 m/s, corresponding effective degree of saturation profiles are evaluated and plotted against the measured data as shown in Fig. 14c. The validation results show the predictions from the proposed model agrees very well with the experimental data (Fig. 14c). The RMSE values for the two sets of validation data are calculated to be 0.14 and 0.06.

Song et al. (2014) tested Fontainebleau sand at a dry unit mass of 1.7 Mg/m^3 in a 300 mm thick environmental chamber. Various sensors were installed for measuring temperature, water content, and matric suction at different depths. Song et al. (2014) used the water vapor balance method, which relies on humidity and airflow rate, to determine the evaporation rate from the environmental chamber. Fig. 15a, c, and d show the predicted and measured SWRCs, effective degree of saturation, and matric suction profiles for Fontainebleau sand, respectively. As seen, a very good match with the measured data can be obtained from the proposed derivation. Using the fitted SWRC parameters (see Fig. 15a), temperature profiles (see Fig. 15b), evaporative fluxes (see Fig. 15c), and the saturated hydraulic conductivity of k_s = 1.69E-08 m/s, the effective degree of saturation, and matric suction profiles are evaluated and plotted against the measured data (Fig. 15c and d). The RMSE values of the predicted effective degree of saturation profiles and matric suction profiles of Fontainebleau sand data are found to be 0.07 and 0.1 and 4.2 kPa and 7.8 kPa for two evaporative fluxes, respectively.

As noted from the results in Figs. 14 and 15, the predictive accuracy of the proposed formulations decreases near the ground surface. This lower accuracy near the surface may be the result of vapor diffusion being a dominant factor, which is not considered in the current study. Vapor diffusion is primarily controlled by the availability of air-filled voids. During evaporation, there is less liquid water in the void space, which increases air-filled voids facilitating vapor flux in the near surface zone (e.g., Bittelli et al., 2008; An et al., 2017). The vapor flux becomes less dominant as the depth increases below the surface. Another possible factor causing the differences between the modeled and measured data in Figs. 14 and 15, especially at the top, can be due to different flow

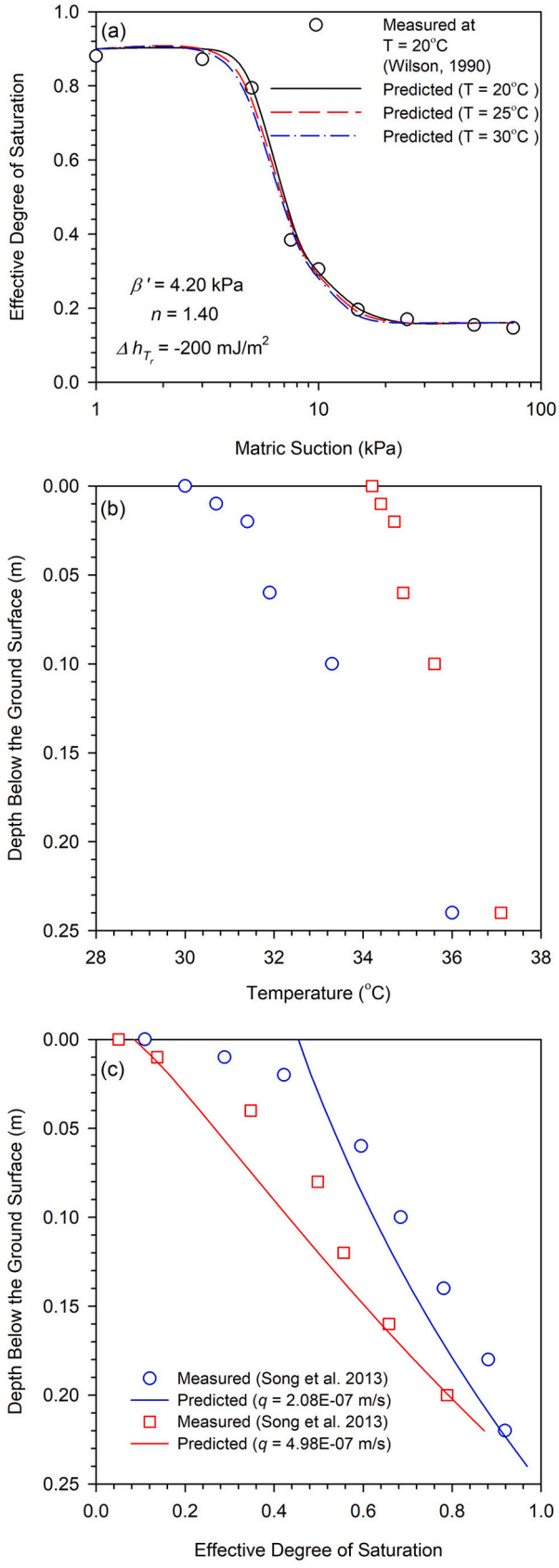

Fig. 14. Comparison of measured (Wilson, 1990) and predicted data (current study) for Beaver Creek sand: (a) soil water retention curve, (b) measured temperature profiles, and (c) effective degree of saturation depth profile for two evaporation conditions.

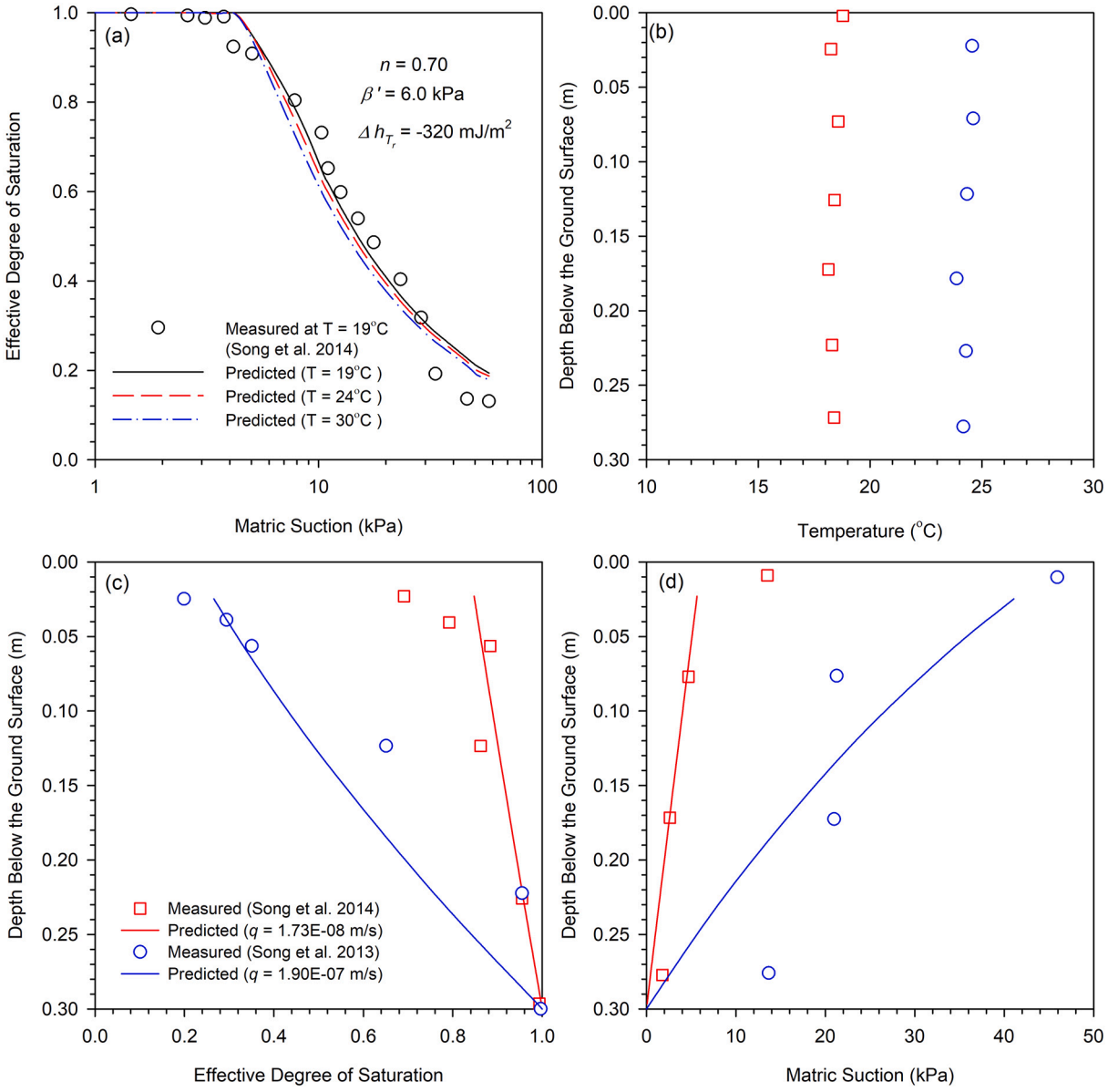

Fig. 15. Comparison of measured (Song et al., 2014) and predicted data (current study) for Fontainebleau sand: (a) soil water retention curve, (b) measured temperature profiles, (c) effective degree of saturation depth profile, and (d) matric suction depth profile for two evaporation conditions.

conditions applied in the test set up versus that assumed in the current analytical derivation. The model prediction improves as we move away from the ground surface and towards the saturation state, where the liquid flow is more dominant compared to vapor flow, which is incorporated in the current study.

The presented framework can be employed to examine the long-term stability of unsaturated slopes (natural and man-made) under concurrent variations in water content and temperature. For instance, prolonged droughts can take up to several years subjecting surface and near surface unsaturated soils to a combination of low water contents and high temperatures over a long period. The presented methodology offers a robust yet practical tool to analyze the stability of natural and man-made slopes under such conditions. To the best of the authors' knowledge, this study is the first attempt in the literature developing an analytical framework for performing stability analysis of unsaturated slopes while accounting for concurrent changes in water content and temperature. The results showed that, under drained conditions, elevated temperatures increase the stability of unsaturated intact slopes. This trend is consistent with the field observations and future predictions reported in the literature. Coe (2012) predicted a decrease in the landslide activity in Slumgullion of Colorado, primarily due to forecasted increases in surface temperature and decreases in precipitation over the next century in this region. Bennett et al. (2016) used aerial photograph analysis, satellite interferometry, and satellite pixel tracking to examine the effect of California's historic 2012–2015 drought on 98 slow-moving landslides in Northern California. Their study showed that the historic drought put the brakes on these landslides. Bennett et al. (2016) concluded that the drought decelerates the earthflow, slowdowns the landslide motion, and reduces the frequency of slope failure (Bennett et al., 2016; Mackey and Roering, 2011). In a follow-on study, Handwerger et al. (2019) employed aerial imagery to examine the post-drought landslide activities in Northern California and found significant increases in activities of slow-moving landslides in 2017, right after the end of the historic drought. Nereson and Finnegan (2019) used historical aerial imagery data (1937–2017) to understand the Oak Ridge earthflow motion and reported the velocity of landslides to decrease during the drought events. Elevated temperatures and moisture deficit associated with the drought increase the suction, which in turn increases the shear

strength and the FOS of intact unsaturated slopes.

This study examined the influence of temperature on the stability of unsaturated intact slopes. The results showed that elevated temperatures have a positive impact on the FOS of slopes under drained heating and mechanical loading conditions. However, elevated temperatures and drying-wetting cycles can possibly trigger the formation of desiccation cracks in fine-grained soils. Desiccation cracks form on the surface but can propagate to several meters below the ground surface. Cracks can adversely affect the integrity and stability of unsaturated slopes and earthen structures by decreasing the soil mass strength, increasing the hydraulic conductivity and inducing preferred pathways for water infiltration, leading to abrupt losses of suction and generation of the excess pore-water pressure during rainfalls (Vahedifard et al., 2014; Abdollahi et al., 2021). Tensile strength, which is the key soil property reinstating the formation of desiccation cracks, is shown to decrease under elevated temperatures (Salimi et al., 2021a, 2021b). Previous studies (Tang et al., 2008, 2010) have revealed that subjecting unsaturated clayey soils to elevated temperatures leads to the development of surface tensile stress and desiccation cracks at higher rates. Salimi et al. (2021a) performed a set of laboratory tests to examine the effect of temperature on the tensile strength during desiccation of two compacted clays with medium to high plasticity. Their results showed that, at the optimum water content, the tensile strength reduced by 36% and 27% in the highly plastic clay and the medium plastic clay, respectively, when the temperature elevated from 20 °C to 60 °C. Further, elevated temperatures can alter the stability of unsaturated slopes through thermal induced changes in vegetation cover (Jamalinia et al., 2019, 2020). In future studies, the proposed slope stability analysis framework can be further extended to incorporate the effect of temperature on cracking and vegetation and the subsequent changes on the stability of slopes.

5. Conclusions

This study aimed to present an analytical framework to quantify the impact of elevated temperatures on the stability of infinite unsaturated intact slopes under different flow conditions. This framework is built based upon the suction stress-based effective stress by considering the temperature dependency of the soil-water retention curve (SWRC) and effective stress. The SWRC model incorporates the thermal effect on the surface tension, contact angle, and enthalpy of immersion.

Matric suction, effective degree of saturation, apparent cohesion, shear strength, and the FOS at temperatures of 25, 40, and 55 °C were studied for three hypothetical soils under hydrostatic, infiltration, and evaporation conditions. The results revealed the changes in all the properties considered with elevated temperatures. The shear strength and FOS trend with temperature for clay and silt soils appear to be monotonic. However, the sand exhibited a non-monotonic behavior. This could be due to the absence of physicochemical forces around the soil interparticle in sands. Further, this could be attributed to the range of variation within the SWRC for the studied sandy slope in which a considerable desaturation reduced the matric suction greatly. The results also illustrated that temperature could have a significant effect on shear strength and thereby the stability of fine-grained soil slopes. The impact of temperature on the shear strength and the FOS is minimal in the case of intact sand slope. The proposed framework is validated against two sets of laboratory data reported in the literature. It is noted that the proposed models able to predict the measured values with a reasonable accuracy.

Though the results showed that elevated temperatures have a positive effect on the long-term FOS of the slope, the negative effect can be caused by the formation of cracks due to tensile stresses developed due to elevated temperatures and loss of vegetation. In future studies, the proposed stability analysis framework can be further extended to incorporate the effect of temperature on cracking and vegetation and then the stability of slopes. This study focused on the stability of slopes under steady-state conditions, which can be representative of the long-term behavior of unsaturated slopes during and after prolonged droughts (or other long-term conditions). A common type of drought-induced slope failure occurs when the drought season is superimposed or followed by heavy rainfall. For tackling such short-term slope stability problems, the presented methodology can be extended by incorporating transient flow conditions.

Declaration of Competing Interest

None.

Acknowledgments

This material is based upon work supported in part by the National Science Foundation under Grant No. CMMI-1634748. Any opinions, findings, and conclusions or recommendations expressed in this material are those of the authors and do not necessarily reflect the views of the National Science Foundation. The authors would like to thank Dr. Toan Duc Cao for his assistance and contributions in the earlier stages of this study.

Appendix A. Derivation of temperature-dependent suction stress profiles under steady flow

Lu and Griffiths (2004) developed an analytical solution for steady-state suction stress profiles versus depth. In this Appendix, we present detailed derivation on the extension of the Lu and Griffiths (2004) formulation to temperature-dependent conditions.

For one-dimensional vertical flow in isotropic and homogenous materials, Darcy's law connects the total potential gradient and flow rate q by:

$$q = -k\left(\frac{dh_t}{dz}+1\right) \tag{25}$$

where k is the hydraulic conductivity depends on the pressure head, $h_t = -\psi/\gamma_w$. The hydraulic conductivity and matric suction can be described by the Gardner (1958) hydraulic conductivity function and the Brooks and Corey (1964) SWRC model, respectively, as:

$$k = k_s exp(\beta' h_t) = k_s\left(\frac{\theta}{\theta_s}\right)^n \tag{26}$$

By substituting Eq. 26 into Eq. 25, we can arrive at a closed-form solution for matric suction profile as follows:

$$q = -k_s exp(\beta' h_t)\left(\frac{dh_t}{dz}+1\right) \tag{27a}$$

$$-\frac{q}{k_s}dz = e^{\beta' h_t}dh + e^{\beta' h_t}dz \tag{27b}$$

Exercising the variable separable method and integrating the above equation by assuming zero suction at the water table, we get:

$$\int_0^z dz = -\int_0^{h_t} \frac{e^{(\beta' h_t)}}{e^{(\beta' h_t)} + q/k_s} dh_t \tag{28}$$

$$\beta' z = -ln\left(\frac{e^{(\beta' h_t)} + q/k_s}{1 + q/k_s}\right) \tag{29}$$

Simplifying the above equation and writing the profile equation for the pressure head, one can obtain:

$$h_t = \frac{1}{\beta'} ln\left[\left(1 + q/k_s\right)e^{-\beta' z} - q/k_s\right] \tag{30}$$

By using the pressure head and matric suction relation, Eq. 30 is then modified in terms of matric suction (ψ) as follows:

$$\psi = \frac{\gamma_w}{\beta'} ln\left[\left(1 + q/k_s\right)e^{-\beta' z} - q/k_s\right] \tag{31}$$

The above equation is defined at the reference temperature. Using the temperature-dependent matric suction (Eq. 5), Eq. 31 can be extended to temperature-dependent conditions as:

$$\psi = \frac{\gamma_w}{\beta'} ln\left[\left(1 + q/k_s\right)e^{-\beta' z} - q/k_s\right]\left(\frac{\beta_{T_r} + T_r}{\beta + T}\right) \tag{32}$$

To determine the steady-state effective degree of saturation profile under elevated temperatures, one can substitute Eqs. 5 and 31 into Eq. 10 to reach:

$$\left(\frac{\theta}{\theta_s}\right) = S_e = \left\{exp\left[ln\left(\left(1 + q/k_s\right)e^{-\beta' z} - q/k_s\right)\left(\frac{\beta_{T_r} + T_r}{\beta + T}\right)\right]\right\}^{1/n} \tag{33}$$

References

Abdollahi, M., Vahedifard, F., Abed, M., Leshchinsky, B.A., 2021. Effect of tension crack formation on active earth pressures encountered in unsaturated retaining wall backfills. J. Geotech. Geoenviron. https://doi.org/10.1061/(ASCE)GT.1943-5606.0002434.

Alsherif, N.A., McCartney, J.S., 2015. Thermal behaviour of unsaturated silt at high suction magnitudes. Geotechnique 65 (9), 703–716.

An, N., Hemmati, S., Cui, Y., 2017. Numerical analysis of soil volumetric water content and temperature variations in an embankment due to soil-atmosphere interaction. Comput. Geotech. 83, 40–51.

Başer, T., Dong, Y., Moradi, A.M., Lu, N., Smits, K., Ge, S., Tartakovsky, D., McCartney, J. S., 2018. Role of nonequilibrium water vapor diffusion in thermal energy storage systems in the vadose zone. J. Geotech. Geoenviron. 144 (7), 04018038.

Behbehani, F. and McCartney, J.S. (2020). "Impacts of unsaturated conditions on the ultimate axial capacity of energy piles. EUnsat 2020: The 4th European Conference on Unsaturated Soils. Lisbon, Portugal. Jun. 24–26. E3S Web Conf., Paris. Vol. 195, 04005. pp. 1–6. DOI: doi:https://doi.org/10.1051/e3sconf/202019504005.

Bennett, G.L., Roering, J.J., Mackey, B.H., Handwerger, A.L., Schmidt, D.A., Guillod, B. P., 2016. Historic drought puts the brakes on earthflows in Northern California. Geophys. Res. Lett. 43 (11), 5725–5731.

Bishop, A.W., 1959. The principle of effective stress. Teknisk ukeblad 39, 859–863.

Bittelli, M., Ventura, F., Campbell, G.S., Snyder, R.L., Gallegati, F., Pisa, P.R., 2008. Coupling of heat, water vapor, and liquid water fluxes to compute evaporation in bare soils. J. Hydrol. 362 (3–4), 191–205.

Bo, M.W., Fabius, M., Fabius, K., 2008. Impact of global warming on stability of natural slopes. In: *Proceedings of the 4th Canadian Conference on Geohazards: From Causes to Management, Presse de Univ.* Laval, Quebec.

Brooks, R.H., Corey, A.T., 1964. Hydraulic properties of porous media: Hydrology paper no. 3. Colorado State Univ, Fort Collins, CO.

Burghignoli, A., Desideri, A., Miliziano, S., 2000. A laboratory study on the thermomechanical behaviour of clayey soils. Can. Geotech. J. 37 (4), 764–780.

Campanella, R.G., Mitchell, J.K., 1968. Influence of temperature variations on soil behaviour. J. Soil Mech. Foundat. Div. ASCE 94, 704–734.

Cao, T.C., Thota, S.K., Vahedifard, F., Amirlatifi, A., 2021. A temperature-dependent model for thermal conductivity function of unsaturated soils. In: *Proc. 2021 International Foundations Congress and Equipment Exposition, IFCEE 2021*, Dallas, TX, May 10–14, 2021, Geotechnical Special Publication No. 325, Reston, VA, pp. 89–98. https://doi.org/10.1061/9780784483428.010.

Chiang, F., Mazdiyasni, O., AghaKouchak, A., 2021. Evidence of anthropogenic impacts on global drought frequency, duration, and intensity. Nature communications 12 (1), 1–10.

Chowdhury, R.H., Azam, S., 2016. Unsaturated shear strength properties of a compacted expansive soil from Regina, Canada. Innovat. Infrastruct. Solut. 1 (1), 47.

Coccia, C.J., Gupta, R., Morris, J., McCartney, J.S., 2013. Municipal solid waste landfills as geothermal heat sources. Renew. Sust. Energ. Rev. 19, 463–474.

Coe, J.A., 2012. Regional moisture balance control of landslide motion: Implications for landslide forecasting in a changing climate. Geology 40 (4), 323–326.

Constantz, J., 1982. Temperature Dependence of Unsaturated Hydraulic Conductivity of two Soils 1. Soil Sci. Soc. Am. J. 46 (3), 466–470.

Cui, Y.J., Tang, A.M., Loiseau, C., Delage, P., 2008. Determining the unsaturated hydraulic conductivity of a compacted sand–bentonite mixture under constant-volume and free-swell conditions. Phys. Chem. Earth, Parts A/B/C 33, S462–S471.

Damiano, E., Mercogliano, P., 2013. Potential Effects of Climate Change on Slope Stability in Unsaturated Pyroclastic Soils. In: Landslide Science and Practice (Pp. 15–25). Springer, Berlin, Heidelberg.

Dorsey, N.E., 1940. Properties of Ordinary Water Substance. Reinhold, New York.

Duncan, J.M., Wright, S.G., 2005. Soil Strength and Slope Stability, 297 Pp. John Wiley, Hoboken, N. J.

Elia, G., Cotecchia, F., Pedone, G., Vaunat, J., Vardon, P.J., Pereira, C., Josifovski, J., 2017. Numerical modelling of slope–vegetation–atmosphere interaction: an overview. Q. J. Eng. Geol. Hydrogeol. 50 (3), 249–270.

Gardner, W.R., 1958. Steady state solutions of the unsaturated moisture flow equation with application to evaporation from a water table. Soil Sci. 85, 228–232.

Garrido, C., Otero, A.F., Cidras, J., 2003. Theoretical model to calculate steady-state and transient ampacity and temperature in buried cables. IEEE Transact. Power Deliv. 18 (3), 667–678.

Godt, J.W., Baum, R.L., Lu, N., 2009. Landsliding in partially saturated materials. Geophys. Res. Lett. 36 (2).

Godt, J.W., Şener-Kaya, B., Lu, N., Baum, R.L., 2012. Stability of infinite slopes under transient partially saturated seepage conditions. Water Resour. Res. 48 (5).

Goodman, C.C., Vahedifard, F., 2019. Microstructural Evaluation of Clay at Elevated Temperatures. Géotech. Letters 9 (3), 225–230.

Graham, J., Tanaka, N., Crilly, T., Alfaro, M., 2001. Modified Cam-Clay modelling of temperature effects in clays. Can. Geotech. J. 38 (3), 608–621.

Grant, S.A., 2003. Extension of a temperature effects model for capillary pressure saturation relations. Water Resour. Res. 39 (1). SBH-1.

Grant, S.A., Salehzadeh, A., 1996. Calculation of temperature effects on wetting coefficients of porous solids and their capillary pressure functions. Water Resour. Res. 32 (2), 261–270.

Greenway, D.R., 1987. Vegetation and slope stability. Slope Stability 187–230.

Haar, L., Gallagher, J.S., Kell, G.S., 1984. NBS/NRC Steam Table. Hemisphere Publishing Corporation, New York.

Handwerger, A.L., Fielding, E.J., Huang, M.H., Bennett, G.L., Liang, C., Schulz, W.H., 2019. Widespread initiation, reactivation, and acceleration of landslides in the

northern California Coast Ranges due to extreme rainfall. J. Geophys. Res. Earth Surf. 124 (7), 1782–1797.
Houston, S.L., Houston, W.N., Williams, N.D., 1985. Thermo-mechanical behavior of seafloor sediments. J. Geotech. Eng. 111 (11), 1249–1263.
Hueckel, T., Baldi, G., 1990. Thermoplasticity of saturated clays: Experimental constitutive study. J. Geotech. Eng. 116 (12), 1778–1796.
Hueckel, T., Pellegrini, R., Del Olmo, C., 1998. A constitutive study of thermo-elasto-plasticity of deep carbonatic clays. Int. J. Numer. Anal. Methods Geomech. 22 (7), 549–574.
Jafari, N.H., Stark, T.D., Thalhamer, T., 2017. Progression of elevated temperatures in municipal solid waste landfills. J. Geotech. Geoenviron. 143 (8), 05017004.
Jamalinia, E., Vardon, P.J., Steele-Dunne, S.C., 2019. The effect of Soil-Vegetation-Atmosphere interaction: a numerical study. Environ. Geotechn. https://doi.org/10.1680/jenge.18.00201.
Jamalinia, E., Vardon, P.J., Steele-Dunne, S.C., 2020. The impact of evaporation induced cracks and precipitation on temporal slope stability. Comput. Geotech. 122, 103506. https://doi.org/10.1016/j.compgeo.2020.103506.
Kasozi, A.M., Siddharthan, R.V., Mahamud, R., 2015. Temperature distribution in mechanically stabilized earth wall soil backfills for design under elevated temperature conditions. J. Ther. Sci. Eng. Applicat. 7 (2), 021004.
Kuntiwattanakul, P., Towhata, I., Ohishi, K., Seko, I., 1995. Temperature effects on undrained shear characteristics of clay. Soils Found. 35 (1), 147–162.
Laguros, J.G., 1969. Effect of temperature on some engineering properties of clay soils. Highway Res. Board Spe. Rep. 103.
Li, C., Kong, G., Liu, H., Abuel-Naga, H., 2019. Effect of temperature on behaviour of red clay–structure interface. Can. Geotech. J. 56 (1), 126–134.
Lide, D.R., 1995. Handbook of Chemistry and Physics, 75th edn. CRC Press, New York.
Likos, W., Lu, N., Godt, J., 2014. Hysteresis and uncertainty in Soil Water-Retention Curve Parameters. J. Geotech. Geoenviron. Eng. 140 (4), 04013050.
Lingnau, B.E., Graham, J., Yarechewski, D., Tanaka, N., Gray, M.N., 1996. Effects of temperature on strength and compressibility of sand-bentonite buffer. Eng. Geol. 41 (1–4), 103–115.
Lorenz, R., Jaeger, E.B., Seneviratne, S.I., 2010. Persistence of heat waves and its link to soil moisture memory. Geophys. Res. Lett. 37 (9).
Lu, N., Dong, Y., 2015. Closed-form equation for thermal conductivity of unsaturated soils at room temperature. J. Geotech. Geoenviron. Eng. 141 (6), 04015016.
Lu, N., Godt, J., 2008. Infinite slope stability under steady unsaturated seepage conditions. Water Resour. Res. 44 (11), W11404.
Lu, N., Griffiths, D.V., 2004. Suction stress profiles in unsaturated soils. J. Geotech. Geoenviron. Eng. 130 (10), 1063–1076.
Lu, N., Likos, W.J., 2004. Unsaturated Soil Mechanics. Wiley, Hoboken, NJ.
Lu, N., Likos, W.J., 2006. Suction stress characteristic curve for unsaturated soil. J. Geotech. Geoenviron. Eng. 132 (2), 131–142.
Lu, N., Godt, J.W., Wu, D.T., 2010. A closed-form equation for effective stress in unsaturated soil. Water Resour. Res. 46 (5).
Mackey, B.H., Roering, J.J., 2011. Sediment yield, spatial characteristics, and the long-term evolution of active earthflows determined from airborne LiDAR and historical aerial photographs. Eel River, California. Geol. Soc. Am. Bull. 123 (7–8), 1560–1576.
Maghsoodi, S., Cuisinier, O., Masrouri, F., 2019. Thermal effects on the mechanical behaviour of the soil-structure interface. Can. Geotech. J. https://doi.org/10.1139/cgj2018-0583.
Mašín, D., Khalili, N., 2011. Modelling of thermal effects in hypoplasticity. In: Proceedings of the 13th International Conference of the IACMAG, Melbourne, Australia, Vol. 1, pp. 237–245.
Mazdiyasni, O., AghaKouchak, A., 2015. Substantial Increase in Concurrent Droughts and Heatwaves in the United States. In: Proc., the Natl. Acad. of Sci, 112(37), pp. 11484–11489.
McCartney, J.S., Jafari, N.H., Hueckel, T., Sanchez, M., Vahedifard, F., 2019. Emerging thermal issues in geotechnical engineering. In: Lu, N., Mitchell, J.K. (Eds.), Geotechnical Fundamentals for Addressing New World Challenges. Springer, pp. 275–317. ISBN: 978-3-030-06249-1.
Mitchell, J.K., 1964. Shearing resistance of soils as a rate process. J. Soil Mech. Foundat. Div. 90, 29–61.
Montgomery, D.R., Dietrich, W.E., 1994. A physically based model for the topographic control on shallow landsliding. Water Resour. Res. 30 (4), 1153–1171.
Mukherjee, S., Mishra, A.K., 2021. Increase in compound drought and heatwaves in a warming world. Geophysical Research Letters 48 (1) e2020GL090617.
Nereson, A.L., Finnegan, N.J., 2019. Drivers of earthflow motion revealed by an 80 yr record of displacement from Oak Ridge earthflow, Diablo Range, California, USA. Bulletin 131 (3–4), 389–402.
Nishimura, S., Martin, C.J., Jardine, R.J., Fenton, C.H., 2009. A new approach for assessing geothermal response to climate change in permafrost regions. Géotechnique 59, 213–227.
Philip, J.R., 1969. Theory of infiltration. In: Advances in Hydroscience, 5. Elsevier, pp. 215–296.
Philip, J.R., De Vries, D.A., 1957. Moisture movement in porous materials under temperature gradients. EOS Trans. Am. Geophys. Union 38 (2), 222–232.
Pillsbury, A.F., 1950. Effects of particle size and temperature on the permeability of sand to water. Soil Sci. 70 (4), 299–300.
Plum, R.L., Esrig, M.I., 1969. Effects of Temperature and Heat on Engineering Behaviour of Soils. Highway Research Board, Washington, DC.
Pradel, D., Raad, G., 1993. Effect of permeability on surficial stability of homogeneous slopes. J. Geotech. Eng. 119 (2), 315–332.
Robinson, J.D., Vahedifard, F., 2016. Weakening mechanisms imposed on California's levees under multiyear extreme drought. Clim. Chang. 137 (1–2), 1–14.
Roshani, P., Sedano, J.A.I., 2016. Incorporating temperature effects in soil water characteristics curves. Indian Geotech. J. 46 (3), 309–318.
Salata, F., Nardecchia, F., de Lieto Vollaro, A., Gugliermetti, F., 2015. Underground electric cables a correct evaluation of the soil thermal resistance. Appl. Therm. Eng. 78, 268–277.
Salimi, K., Cerato, A., Vahedifard, F., Miller, G., 2021a. Tensile strength of compacted clays during desiccation under elevated temperatures. Geotech. Test. J. 44 (4), 1119–1134. https://doi.org/10.1520/GTJ20200114.
Salimi, K., Cerato, A., Vahedifard, F., Miller, G.A., 2021b. A temperature-dependent model for tensile strength characteristic curve of unsaturated soils. Geomech. Energy Environ. 28, 100244. https://doi.org/10.1016/j.gete.2021.100244.
Sedighi, M., Hepburn, B.D.P., Thomas, H.R., Vardon, P.J., 2018. Energy balance at the soil atmosphere interface. Environ. Geotech. 5 (3), 146–157. https://doi.org/10.1680/jenge.15.00054.
She, H.Y., Sleep, B.E., 1998. The effect of temperature on capillary pressure-saturation relationships for air-water and perchloroethylene-water systems. Water Resour. Res. 34 (10), 2587–2597.
Song, W.K., Cui, Y.J., Tang, A.M., Ding, W.Q., Tran, T.D., 2014. Experimental study on water evaporation from sand using environmental chamber. Can. Geotech. J. 51 (2), 115–128.
Tang, C., Shi, B., Liu, C., Zhao, L., Wang, B., 2008. Influencing factors of geometrical structure of surface shrinkage cracks in clayey soils. Eng. Geol. 101 (3–4), 204–217.
Tang, C.S., Cui, Y.J., Tang, A.M., Shi, B., 2010. Experiment evidence on the temperature dependence of desiccation cracking behavior of clayey soils. Eng. Geol. 114 (3–4), 261–266.
Tang, A.M., Hughes, P.N., Dijkstra, T.A., Askarinejad, A., Brenčič, M., Cui, Y.J., Grossi, G., 2018. Atmosphere–vegetation–soil interactions in a climate change context; impact of changing conditions on engineered transport infrastructure slopes in Europe. Q. J. Eng. Geol. Hydrogeol. 51 (2), 156–168.
Thota, S.K., Cao, T.D., Vahedifard, F., Ghazanfari, E., 2019. Stability analysis of an unsaturated silty slope under nonisothermal conditions. In: Geo-Congress 2019: Geotechnical Materials, Modeling, and Testing. American Society of Civil Engineers, Reston, VA, pp. 844–852.
Uchaipichat, A., 2017. Temperature and suction effects on slope stability under undrained condition. Appl. Mech. Mater. Trans Tech Publicat. 858, 98–103.
Uchaipichat, A., Khalili, N., 2009. Experimental investigation of thermo-hydro-mechanical behaviour of an unsaturated silt. Géotechnique 59 (4), 339–353.
Vahedifard, F., Leshchinsky, B.A., Sehat, S., Leshchinsky, D., 2014. Impact of cohesion on seismic design of geosynthetic-reinforced earth structures. J. Geotech. Geoenviron. Eng. ASCE 140 (6), 04014016.
Vahedifard, F., AghaKouchak, A., Robinson, J.D., 2015. Drought threatens California's levees. Science 349 (6250), 799.
Vahedifard, F., Robinson, J.D., AghaKouchak, A., 2016a. Can protracted drought undermine the structural integrity of California's earthen levees? J. Geotech. Geoenviron. Eng. 142 (6), 02516001.
Vahedifard, F., Leshchinsky, D., Mortezaei, K., Lu, N., 2016b. Effective stress-based limit equilibrium analysis for homogeneous unsaturated slopes. Int. J. Geomech. https://doi.org/10.1061/(ASCE)GM.1943-5622.0000554. D4016003.
Vahedifard, F., AghaKouchak, A., Ragno, E., Shahrokhabadi, S., Mallakpour, I., 2017. Lessons from the Oroville dam. Science 355 (6330), 1139–1140.
Vahedifard, F., Williams, J.M., AghaKouchak, A., 2018a. Geotechnical engineering in the face of climate change: role of multi-physics processes in partially saturated soils. In: Proc. IFCEE 2018, GSP No. 295, pp. 353–364.
Vahedifard, F., Cao, T.D., Thota, S.K., Ghazanfari, E., 2018b. Nonisothermal Models for Soil Water Retention Curve. J. Geotech. Geoenviron. Eng. 144 (9), 04018061.
Vahedifard, F., Cao, T.D., Ghazanfari, E., Thota, S.K., 2019. Closed-form models for nonisothermal effective stress of unsaturated soils. J. Geotech. Geoenviron. Eng. 145 (9), 04019053.
Vahedifard, F., Thota, S.K., Cao, T.D., Samarakoon, R.A., McCartney, J.S., 2020. Temperature-dependent model for small-strain shear modulus of unsaturated soils. J. Geotech. Geoenviron. 146 (12), 04020136.
Vardon, P.J., 2015. Climatic influence on geotechnical infrastructure: a review. Environ. Geotech. 2 (3), 166–174.
Wan, M., Ye, W.M., Chen, Y.G., Cui, Y.J., Wang, J., 2015. Influence of temperature on the water retention properties of compacted GMZ01 bentonite. Environ. Earth Sci. 73, 4053–4061.
Watson, K.M., 1943. Thermodynamics of the liquid state. Ind. Eng. Chem. 35 (4), 398–406.
Wilson, G.W., 1990. Soil Evaporative Fluxes for Geotechnical Engineering Problems. Ph. D. Dissertation. University of Saskatchewan, Canada.
Yavari, N., Tang, A.M., Pereira, J.M., Hassen, G., 2016. Effect of temperature on the shear strength of soils and the soil–structure interface. Can. Geotech. J. 53 (7), 1186–1194.
Yesiller, N., Hanson, J.L., 2003. Analysis of temperatures at a municipal solid waste landfill. In: *Proceedings of the 9th international waste management and landfill symposium. October 6–10, 2003*. Cagliari, Italy. 1–10.